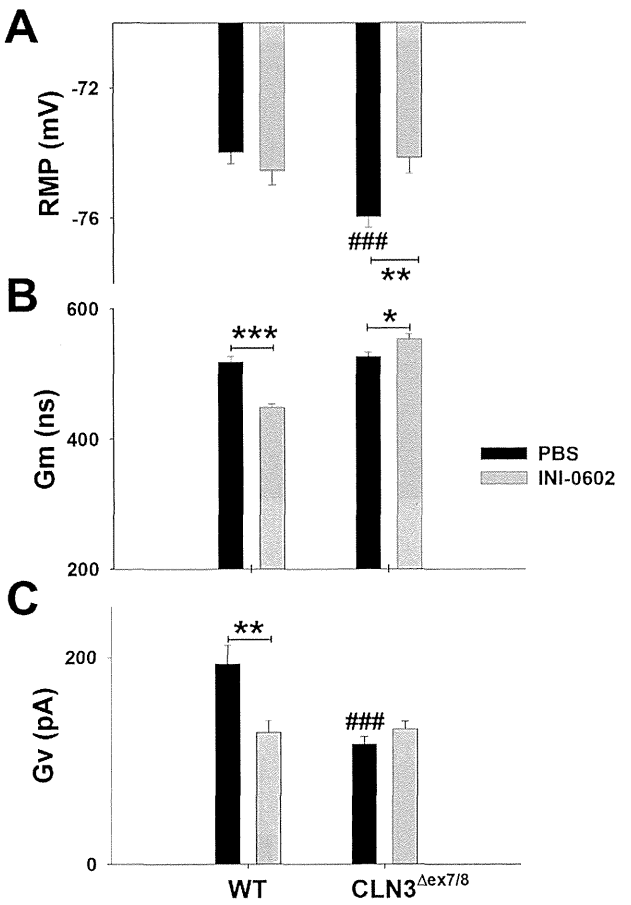

Figure 10. *In vivo* administration of the HC inhibitor INI-0602 alters astrocyte electrophysiological properties. $CLN3^{\Delta ex7/8}$ and wild type (WT) mice (n = 6–9/group) were treated with INI-0602 (10 mg/kg) or PBS from postnatal day 30 to 60, whereupon acute brain slices were prepared to quantitate resting membrane potential (RMP; A), resting membrane conductance (Gm; B), and voltage-dependent membrane conductance (Gv; C) in astrocytes from the somatosensory cortex using whole-cell patch clamp recordings. Significant differences between WT and $CLN3^{\Delta ex7/8}$ astrocytes are denoted by hatched signs (###, $p<0.001$), whereas changes between WT or $CLN3^{\Delta ex7/8}$ mice treated with INI-0602 or PBS are indicated by asterisks (*$p<0.05$; **$p<0.01$; ***$p<0.001$).
doi:10.1371/journal.pone.0095023.g010

synthetase and GLAST expression may also originate from the protein trafficking defects that have been described in JNCL [75,76,77].

Based on the finding that astrocyte HC activity was significantly elevated at postnatal day 30 in $CLN3^{\Delta ex7/8}$ mice, coupled with published reports suggesting that HC opening can be linked with pathology, we treated $CLN3^{\Delta ex7/8}$ mice with the HC inhibitor INI-0602. The rationale for delayed administration at postnatal day 30 was to more closely model the age when a diagnosis of JNCL is made in children. Treatment of $CLN3^{\Delta ex7/8}$ animals with INI-0602 for a 30 day period significantly decreased lysosomal ceroid inclusions in several brain regions. In addition, the "passive" component of membrane conductance in $CLN3^{\Delta ex7/8}$ astrocytes (Gm) was also affected by INI-0602 treatment; however, its "reactive" voltage-dependent component (Gv; Figure 10) was not. The latter agrees with the failure to detect any changes in astrocyte HCs following INI-0602 administration *in vivo*, since Gv is more linked with HC activity than Gm [41]. Another beneficial effect of INI-0602 was its ability to modify resting membrane potential in $CLN3^{\Delta ex7/8}$ astrocytes. Although HC opening in various brain regions of $CLN3^{\Delta ex7/8}$ mice was only transient, it is clear that INI-0602 exerts beneficial effects, which may be explained, in part, by its ability to enhance astrocyte GJC and modify membrane conductance and potential. We found that INI-0602 blocked HC opening in acute brain slices from untreated mice, whereas, surprisingly, no changes in HC activity were observed in slices recovered from animals after a one month treatment period with INI-0602 *in vivo*. This discrepancy could be explained by the short-term actions of INI-0602 in the CNS. Indeed, Takeuchi et. al. reported a steady decline in brain INI-0602 concentrations *in vivo* during the first three hours after injection when the drug was administered to mice every other day, as was done in the current study [68]. In addition, our *in vitro* studies in acute brain slices showed that INI-0602 was easily washed out of brain tissues and, as such, its primary effect (i.e. inhibition of HC activity) is expected to be relatively short-lived. Therefore, the repetitive inhibition of astrocyte HC activity and/or membrane depolarization during the one month treatment period with INI-0602 may cause secondary adaptations in the brains of $CLN3^{\Delta ex7/8}$ mice, resulting in the therapeutic benefits reported here (i.e. reducing lysosomal inclusion burdens). This possibility is supported by the fact that astrocyte GJC was significantly increased following INI-0602 treatment, which, theoretically would occur by HC pairing to form more GJs and/or HC closure. Another option is that INI-0602 may influence pathways that are distinct from HC/GJ. This is suggested by the fact that CBX, the parental compound from which INI-0602 was derived, possesses other effects besides regulating GJ/HC activity [78,79,80] and was only partially capable of blocking INI-0602 action in acute brain slices (Figure 8B). Indeed, the changes in astrocytic membrane potential and conductance evoked by INI-0602 in brain slices are expected to influence other cellular functions in the CNS. An alternative explanation is that INI-0602 changes membrane fluidity and/or alters the trafficking patterns of molecules that improve disease outcomes, attributes that are consistent with other GJ/HC inhibitors [81,82]. By extension, INI-0602 may slow HC diffusion in the lipid bilayer to facilitate the docking of HCs on neighboring astrocytes and/or promote HC trafficking to the plasma membrane, both of which would facilitate the establishment of GJ channels. This possibility agrees with our findings that astrocyte GJC was significantly increased in both WT and $CLN3^{\Delta ex7/8}$ astrocytes following a one month treatment period with INI-0602; however, future studies outside the scope of the current report are needed to support this mechanism of action. A final option emanates from the finding that $CLN3^{\Delta ex7/8}$ astrocyte HC activity declines over time. Since mice were 60 days-old following the one month dosing period with INI-0602, the natural HC closure observed in untreated $CLN3^{\Delta ex7/8}$ mice could account for the inability to detect a major effect with INI-0602 treatment, since a large majority of HCs were already closed. However, the fact that INI-0602 significantly increased GJC in both $CLN3^{\Delta ex7/8}$ and WT astrocytes implies that the drug was still closing HCs, albeit at a level that was not detectable by our *ex vivo* methodology. Although INI-0602 significantly reduced inclusion burdens $CLN3^{\Delta ex7/8}$ mice it did not show any clear effects on glutamate or GABA levels as measured by MR spectroscopy, which may originate from the dosing regimen and/or drug concentration used, age of the animals, and/or length of time mice received the compound. Experiments are ongoing to determine whether long-term INI-

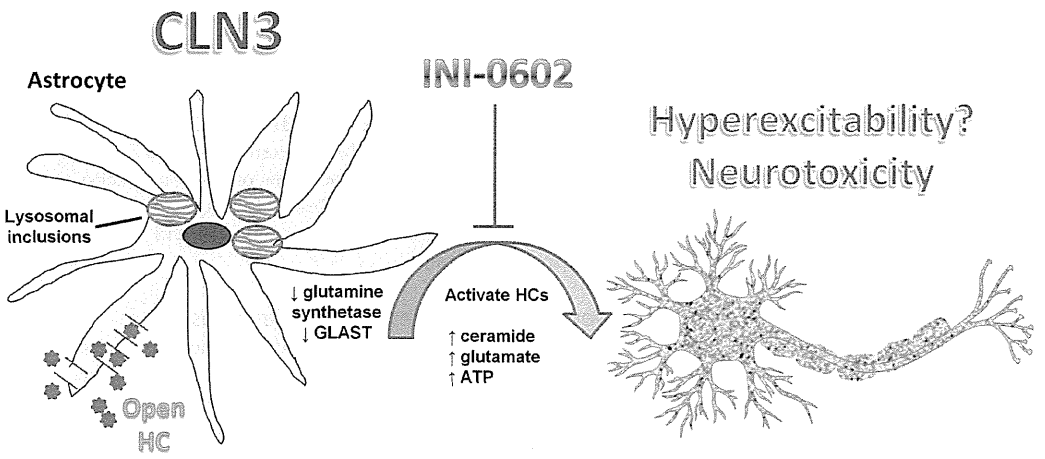

Figure 11. Proposed relationship between astrocyte HC activity, brain metabolites, and neuronal loss in JNCL. Astrocyte HCs are transiently opened in numerous brain regions in the context of CLN3 mutation, which likely distorts the brain metabolome. This is supported by the ability of the HC inhibitor, INI-0602, to reduce lysosomal ceroid inclusions and enhance gap junction communication that is associated with the maintenance of homeostatic gradients in the CNS milieu. Previous studies have reported increases in ceramide, ATP, and glutamate in JNCL, the latter of which can be linked to HC action as well as the global decreases in glutamine synthetase and GLAST expression in $CLN3^{\Delta ex7/8}$ mice. Collectively, these changes are suggestive of progressive loss of normal astrocyte homeostatic functions, which may contribute to neuronal loss in JNCL.
doi:10.1371/journal.pone.0095023.g011

0602 treatment can limit neuronal death observed at advanced ages in $CLN3^{\Delta ex7/8}$ animals (i.e. 6–8 months).

Previous work from us and others has shown a reciprocal relationship between GJC and HC activity in the context of injury or inflammation [41,42]. In general, pathological disturbances lead to reduced astrocyte GJC and a concomitant opening of HCs, which is thought to be attributed, in part, to the action of proinflammatory mediators [25,26]. In the current report, increased HC activity was observed in the S1C of $CLN3^{\Delta ex7/8}$ mice at postnatal day 30, which correlated with a trend towards decreased GJC in the same region. Likewise, HC activity was significantly decreased in the HPC at postnatal day 90, which correlated with increased GJC in this same location. Nonetheless, it appears too simplistic to expect changes in GJC to always parallel HC function, particularly given the vast differences in cell types and complexity in various brain regions. We propose that the increase in GJC observed in $CLN3^{\Delta ex7/8}$ mice may represent a compensatory response to failing astrocyte "health" as demonstrated by the decreased glutamine synthetase and GLAST expression reported here in the face of elevated glutamate levels in the JNCL brain as described by other groups [53,59,61]. Importantly, we found that GFAP expression was significantly elevated in $CLN3^{\Delta ex7/8}$ mice at postnatal day 90 in the VC, HPC, and TH in agreement with previous reports from other laboratories in CLN3 mutant mice [8,20]. This is a key observation, since it indicated that the decreases in Cx43, GLAST, and glutamine synthetase detected in $CLN3^{\Delta ex7/8}$ animals did not result from astrocyte loss. Rather, these findings reveal the attrition of molecules that regulate glutamate homeostasis, which likely triggers astrocyte activation in an attempt to compensate for this decline. It remains to be determined whether these GFAP-reactive astrocytes exert a beneficial or detrimental response in the context of disease progression. It was surprising that Cx43 and Cx30 staining were both reduced at postnatal day 90, yet astrocyte GJC was unaffected. A potential explanation for this observation is that abundant Cx43 and Cx30 protein still remained, which was likely sufficient to maintain functional GJ channels, particularly since HC activity was dramatically decreased at postnatal day 90 in several brain regions of CLN3 mutant animals. Alternatively, it is possible that CLN3 mutation leads to a redistribution in Cx43 and/or Cx30 that favors GJ plaque formation rather than unopposed HCs. This could conceivably result from increased homing of Cxs to GJ plaques and/or impaired plaque turnover. In addition, astrocytes have been reported to express Cx26 [83], which could compensate for the reductions in Cx43 and Cx30 observed in $CLN3^{\Delta ex7/8}$ animals. Finally, pannexin proteins are also expressed by astrocytes and form HCs [84,85]. It is possible that pannexin levels are altered in $CLN3^{\Delta ex7/8}$ mice, which may account for some of the differences in HC activity observed in the current study. The reduction in Cx43 expression was congruent with decreases in glutamine synthetase and GLAST levels in $CLN3^{\Delta ex7/8}$ mice that were more profound in comparison, suggestive of a generalized decline in astrocyte homeostasis. Future studies examining these parameters in older $CLN3^{\Delta ex7/8}$ animals will reveal whether these changes are progressive and, if so, they could conceivably augment neuronal pathology and eventual cell death.

In conclusion, our study has identified a novel decline in astrocyte function over the first three postnatal months in $CLN3^{\Delta ex7/8}$ mice. Impairments in astrocyte homeostatic effects, as suggested by the dramatic reduction in glutamine synthetase and GLAST expression in $CLN3^{\Delta ex7/8}$ animals, can compromise neuronal function and conceivably impact neuronal demise during JNCL. We also observed widespread opening of astrocyte HCs in numerous brain regions, which although transient, could set the stage for downstream pathological effects. Indeed, targeting early changes in astrocyte HC function in the $CLN3^{\Delta ex7/8}$ brain with the CBX derivative INI-0602 led to reductions in lysosomal ceroid inclusions. The exact mechanisms whereby INI-0602 provides these beneficial effects remain to be elucidated; however, its ability to enhance astrocyte GJC and modify membrane properties are likely candidates based on the ability of astrocyte syncytia to detoxify glutamate within the CNS. Nevertheless, INI-0602 appears to represent an attractive candidate for further development in the context of JNCL therapeutics.

Materials and Methods

Ethics Statement

This study was conducted in strict accordance with the recommendations in the Guide for the Care and Use of Laboratory Animals of the National Institutes of Health. The protocol was approved by the Institutional Animal Care and Use Committee of the University of Nebraska Medical Center (Approval ID: 11-074-08-EP).

Mice

$CLN3^{\Delta ex7/8}$ mice (C57BL/6 background) that lack a 1.02 kb segment spanning exons 7 and 8 of *CLN3* were used [52]. This represents the most common mutation in ~85% JNCL patients and $CLN3^{\Delta ex7/8}$ mice phenocopy several aspects of JNCL, including neuronal loss, glial activation, metabolic disturbances, and progressive storage material deposition [4,52,86,87]. Age- and sex-matched C57BL/6 mice were used as WT controls (The Jackson Laboratory, Bar Harbor, ME). Both male and female mice were utilized for these studies and no gender influences on experimental outcomes were observed. To analyze early pathological changes during JNCL, $CLN3^{\Delta ex7/8}$ and WT mice (n = 54 and 48, respectively) were evaluated at postnatal days 30–37, 60–67, and 90–97 (referred to throughout the study as postnatal days 30, 60, and 90, respectively). In experiments to quantitate ceroid inclusions, tissues from 12–16 month-old mice were included for comparisons with younger animals.

In some experiments, GFAP-GFP transgenic mice, where GFP expression is driven by the human GFAP promoter (8–12 weeks of age; The Jackson Laboratory) [88], were used to confirm astrocyte staining specificity with CellTracker Blue CMAC (CTB; Invitrogen, San Diego, CA).

In vivo Administration of the HC Inhibitor INI-0602

In some experiments, $CLN3^{\Delta ex7/8}$ and WT mice were treated with the blood-brain barrier permeable CBX analog INI-0602 [68] to determine the functional importance of astrocyte HC activity in disease pathogenesis. $CLN3^{\Delta ex7/8}$ and WT mice received i.p. injections of PBS or 10 mg/kg INI-0602 every other day from postnatal days 30 to 60 (n = 6–17 per group), a dosing regimen that was optimal at reducing clinical symptoms in mouse models of ALS and AD [68]. At the end of the 30 day treatment period, mice were subjected to magnetic resonance (MR) spectroscopy to quantitate the brain metabolome, whereupon they were sacrificed and tissues utilized for subsequent studies. Blood was collected from $CLN3^{\Delta ex7/8}$ and WT mice treated with INI-0602 or vehicle upon sacrifice, whereupon blood chemistry profiles were evaluated using a VetScan2 blood analyzer (Abaxis, Union City, CA; Comprehensive Diagnostic Profile rotor #500-1038).

Magnetic Resonance (MR) Spectroscopy

To evaluate the impact of INI-0602 treatment on the CNS metabolome, MR spectroscopy scanning was conducted on $CLN3^{\Delta ex7/8}$ and WT mice following the one month INI-0602 dosing interval. Briefly, animals were anesthetized with 1.5% isoflurane in a 70% nitrous oxide/30% oxygen mixture and positioned in a custom-made stereotactic holder equipped with a MRI-compatible physiological monitoring system (Model 1025, SA Instruments, Stony Brook, NY). Core body temperature of anesthetized animals was maintained by a warm air delivery system and MR spectroscopy data was obtained using a Bruker Avance 7 Tesla/21 cm small bore system (Billerica, MA) and a lab-built birdcage coil designed for mouse brain imaging. The initial setup for magnetic resonance imaging (MRI) studies included a 3-plane locator scan, where localization and initial shimming using a novel field mapping method was utilized [89]. Once the mouse was positioned and shimmed, MR spectroscopy spectra were obtained from the HPC of $CLN3^{\Delta ex7/8}$ and WT mice±INI-0602 treatment. MR spectroscopy was acquired using 576 averages with a repetition time of 4000 ms, echo time of 50 ms, and 3 kHz bandwidth. Results from quality assurance (QA) phantoms were used to verify accuracy and random error measurements in mice.

Spectroscopic Processing and Analyses

Spectroscopic data were processed by removal of residual water signal using the HLSVD filter. Spectra from ^1H MR spectroscopy data sets were curve fit in the time domain using the QUantitation based on Quantum ESTimation (QUEST) algorithm [90,91] in jMRUI (Java-based version of the magnetic resonance user interface (MRUI) quantitation package), which fits results to a sum of individual metabolite spectra (basis set). Spectra for the basis set were acquired from QA phantoms with the same acquisition parameters used *in vivo*. Phantoms containing either alanine, aspartate, choline, creatine, gamma-amino butyric acid, glutamate, glutamine, glycerophosphocholine, glycine, lactate, myo-inositol, NAA, or taurine were maintained at 38°C using a circulating water bath and buffered to pH 7.4 at physiological osmolarity. Results were normalized to the sum of all 13 metabolites as a semi-quantitative method for reporting metabolite concentrations.

Preparation of Acute Brain Slices and SR101/CTB Staining

To prepare acute brain slices for quantitating astrocyte GJ/HC activity and electrophysiological parameters, $CLN3^{\Delta ex7/8}$ and WT mice were decapitated, whereupon the brains were quickly removed and bathed in ice-cold artificial cerebrospinal fluid (ACSF, in mM: 124 NaCl, 26 $NaHCO_3$, 3 KCl, 2 $MgCl_2$, 2 $CaCl_2$, 0.4 ascorbic acid, 10 glucose) continuously bubbled with carbogen (95% O_2 and 5% CO_2) and maintained at pH, 7.4. Next, 400 μm thick coronal slices were prepared using a Leica VT1000S vibrating-blade microtome (Leica Microsystems, Germany) and immediately placed in ACSF at 32°C. During a 20–30 min incubation period at 32°C, some slices were stained with the astrocyte-selective dye SR101 (400 nM, Sigma-Aldrich, St. Louis, MO) [48] and held in ACSF at room temperature for at least 1 h before use. Other slices were stained with the fluorescent dye CellTracker Blue CMAC (2 μM; Invitrogen) for 30 min in ACSF at room temperature and immediately used for experiments assessing astrocyte HC activity. Brain slices maintained good viability for a 6–8 h period, an interval that was not exceeded in the current study, as demonstrated by stable electrophysiological properties in patched astrocytes across the recording intervals examined. In addition, the CTB dye utilized in these studies was specifically designed to stain live, but not dead cells. By extension, the robust CTB staining reported here provides independent confirmation of cell viability in our acute brain slices. Upon completion of some experiments, CTB-stained brain slices were fixed in 10% formaldehyde and processed according to the histological protocol described below for clarifying the identity of CTB^+ cells.

Brain Regions Examined

To investigate region-dependent changes in astrocyte function in $CLN3^{\Delta ex7/8}$ mice, five brain regions were selected for analysis based on prior reports documenting significant pathology in older animals [6,8,20,52]. These included, layers IV-VI of the primary

somatosensory cortex (S1C); dorsal striatum (STR); layers IV-VI of the primary and secondary areas of the visual cortex (VC); stratum radiatum layer in the CA1 field of the hippocampus (HPC); and ventral posterolateral and posteromedial nuclei of the thalamus (TH). These regions were identified using a mouse brain atlas [92].

Quantification of HC Activity

For assessing astrocyte HC activity, acute brain slices from $CLN3^{\Delta ex7/8}$ and WT mice were pre-stained with CTB to facilitate astrocyte identification and incubated in a submerged chamber while constantly perfused with the HC-permeable dye EtBr (2.5 μM) in ACSF at a rate 1.5 ml/min at 30°C. Z-stack images of CTB and EtBr staining were collected at each of the five brain regions, with 3 random fields of view (FOV) examined for each brain structure. Images were captured at each location every 10 min before EtBr bath application and throughout the 30 min EtBr incubation period. Each image covered a FOV of 167×220 μm and a tissue depth of 55 μm with a total magnification of 400X. Astrocytes were identified by CTB staining with cell bodies marked as regions of interest (ROI), and an average EtBr intensity for each ROI was obtained (designated F) in the same Z-stack where the maximum intensity for CTB was found. Next, EtBr intensity was normalized to background values (F_0) to account for autofluorescent ceroid inclusions, which were taken as the minimal densitometric mean value in the ROI Z-stack, according to the equation: $(F-F_0)/F_0*100\%$. Astrocyte HC activity was calculated as the rate of EtBr uptake in arbitrary units per min (a.u./min) using a linear regression algorithm as previously described [41]. To determine the effect of INI-0602 on astrocyte HC activity and electrophysiological parameters in acute brain slices of $CLN3^{\Delta ex7/8}$ and WT mice, 100 μM INI-0602 was applied to the bath solution during EtBr uptake and electrophysiological measurements.

Electrophysiology

Electrophysiological recordings of astrocytes were performed in the S1C and HPC of acute brain slices from $CLN3^{\Delta ex7/8}$ and WT mice (n = 29/group) as previously described [93]. Acute brain slices were incubated with SR101 to facilitate astrocyte identification. SR101 was utilized in these experiments instead of CTB, since the latter would interfere with AlexaFluor 350 contained in the recording electrode for visualization of astrocyte GJC. Recording electrodes were filled with a solution containing (in mM): 110 K-gluconate, 20 KCl, 0.2 $CaCl_2$, 1 $MgCl_2$, 5 EGTA, and 10 HEPES, pH 7.4 with an electrical resistance of 8–10 MΩ. Whole-cell patch-clamp recordings were performed on astrocytes using a computer-controlled amplifier (Multiclamp 700B, Axon Instruments/Molecular Devices Corp., Sunnyvale, CA) and a video setup. The membrane resistance (Rm) and access resistance (Ra) of astrocytes were calculated using the membrane test function in pClamp-10 (Axon Instruments/Molecular Devices). Resting input conductance (Gm) was calculated by the formula, Gm = Gt *[Rt/Rm], where Rt is total resistance (Rm+Ra) and Gt is total conductance calculated as the linear slope coefficient of the voltage-current relationship (I–V) near the resting membrane potential (RMP, zero holding current). Using this method, cell input conductance (Gi) was calculated at every command voltage (Vc) (on average, from −140 to +60 mV with 5 mV step). All Gi points obtained from 3–4 primary I–V recordings within the Vc range from −90 to −50 mV and RMP range from −90 to −60 mV were included for statistical analysis to evaluate Gm. As observed here and in prior studies, Gi fluctuated over the voltage range and Gi deviation can be associated with voltage-dependent conductance (Gv). In the current report, Gv plot area was calculated using the surveyor's formula for the area of a simple polygon utilizing maximal and minimal Gi points within the Vc range from −90 to 0 mV as determined by the equation:

$$A=\frac{1}{2}\sum_{i=0}^{n-1}[x(i)\times y(i+1)-x(i+1)\times y(i)],$$

where x_i = Vc (mV) and y_i = [Gi - minimal Gi] (nS) on voltage step i from 0 to n-1; A - Gv plot area as the sum of absolute values (mV*nS or pA). To estimate Gv, the 4 maximal [A] values found within 10 consequential I-V recordings were included in the calculation from each recorded cell. Gv should be largely independent from Ra, since membrane potential and conductance used in the formula are oppositely modified in response to Ra changes, as can be concluded from the I-V relationship.

Quantitation of Astrocyte GJC

The GJ permeable dye AlexaFluor 350 (0.5 mM, Invitrogen, San Diego, CA) was included in the patch pipette to visualize the degree of GJC in astrocytes from the S1C or HPC in acute brain slices from $CLN3^{\Delta ex7/8}$ and WT mice after 15–20 min of whole-cell patch-clamp recording. Calculations of astrocyte GJC were performed by enumerating the number of superimposed cell images with AlexaFluor 350 and SR101 fluorescence using appropriate filters in a microscopic FOV of 334×448 μm with a total magnification of 200X. Cell coupling was confirmed by the quantitation of fluorescent intensities using AxioVision software (Zeiss, Germany). Cells were considered GJ coupled if the peak optical intensities for AlexaFluor 350 exceeded 10% of background levels.

Quantitative Measurements of Immunofluorescence Staining and Ceroid Inclusions

For histological analysis, brain slices from $CLN3^{\Delta ex7/8}$ and WT mice were fixed in 10% formaldehyde for 1–2 h, washed in PBS (pH = 7.4), cryoprotected with 30% sucrose overnight, and fast-frozen in OCT embedding medium. Next, 20 μm thick cryostat sections were mounted onto glass slides, air dried, and stored at −20°C until use. Cx43, Cx30, glutamine synthetase, GLAST, and GFAP expression were evaluated in the same five brain regions as HC studies by immunofluorescence staining. Primary antibodies for Cx43 and Cx30 (Molecular Probes/Life Technologies, Carlsbad, CA; #71-0700 and #71-2200, respectively) and glutamine synthetase and GLAST (Abcam, Cambridge, MA; #AB16802 and #AB416, respectively) were visualized using a fluorescein-conjugated secondary antibody (Jackson Immunoresearch Laboratories, West Grove, PA), whereas GFAP (Dako, #20334), MAP2 (Chemicon, Temecula, CA, #AB5622), and Iba-1 (Biocare Medical, #Cp290B) were detected using a biotin-streptavidin approach. Quenching of autofluorescent inclusions in $CLN3^{\Delta ex7/8}$ tissues was achieved by incubating slides with a 70% solution of Sudan Black for 10 min (Figure S2). Tissue sections were imaged using a Carl Zeiss LSM 510 META confocal microscope in a FOV 450×450 μm (200× magnification) or 225×225 μm FOV (400× magnification). Cx43, Cx30, glutamine synthetase, GLAST, and GFAP expression were quantitated using AxioVision software (Zeiss) as the mean intensity staining values (F) normalized to background values in tissue sections where primary antibodies were omitted (F_{bkgr}), i.e. F/F_{bkgr}.

For quantitating autofluorescent ceroid inclusions, images were acquired from live brain slices for each of the five brain regions examined utilizing a GFP filter set (38 HE GFP, EX 470, EM 525;

Zeiss). Each image covered a FOV of 167×220 μm and a tissue depth of 20 μm. Quantitation was performed using AxioVision software with results reported as the area of autofluorescent inclusions (μm^2) for each image.

Western Blot Analysis

Coronal sections (1200 μm thick) were prepared from acute brain slices using a vibratome while bathed in ice-cold ACSF, whereupon the five brain regions described above were manually dissected to collect total protein extracts. Tissues were homogenized in cell lysis buffer [50 mM Tris-HCl, pH 7.5; 150 mM sodium chloride; 0.5% Triton X-100; 1 mM sodium orthovanadate; 10 mM sodium fluoride; 0.5 mM phenylmethanesulfonyl fluoride and supplemented with complete protease inhibitor (Roche, South San Francisco, CA) and phosphatase inhibitor (Thermo Scientific, Waltham, MA) tablets]. Twenty μg of total protein was run on 10% PAGE gels, whereupon Western blotting was performed as previously described [94]. Blots were probed with Cx43 and Cx30 (both from Molecular Probes) and glutamine synthetase and GLAST antibodies (both from Abcam) and developed by chemiluminescence. Blots were stripped and re-probed with an antibody against β-actin (Sigma, St. Louis, MO) to confirm uniformity in gel loading. Blots were quantitated by densitometry analysis using an Alpha Innotech imager (Protein Simple, San Jose, CA), where signals were normalized to β-actin.

Statistical Analyses

A Student's two-tailed *t*-test was used for data analyses (MS Excel 2007), with values reported as the mean ± SEM compiled from independent experiments.

Supporting Information

Figure S1 Age-dependent changes in astrocyte gap junction (GJ) communication in CLN3$^{\Delta ex7/8}$ mice. Acute brain slices were prepared from wild type (WT) and CLN3$^{\Delta ex7/8}$ mice at postnatal days 30, 60 and 90, whereupon the number of GJ coupled astrocytes was evaluated in the somatosensory cortex (S1C) and hippocampus (HPC) by monitoring the passage of the GJ permeable dye AlexaFluor 350 injected in a single astrocyte after whole-cell patch clamp recordings (n = 16–41 astrocytes per group). Significant differences between WT and CLN3$^{\Delta ex7/8}$ astrocytes are denoted by asterisks (*$p<0.05$).
(TIF)

Figure S2 Sudan black quenches the autofluorescence of lysosomal ceroid inclusions in CLN3$^{\Delta ex7/8}$ mice. Cryostat sections (20 μm) were prepared from the somatosensory cortex (S1C) and hippocampus (HPC) of 14 month-old CLN3$^{\Delta ex7/8}$ mice to visualize robust inclusion deposition across multiple wavelengths. Sections were incubated with 10% Sudan Black for 10 min followed by DAPI staining to visualize nuclei.
(TIF)

Figure S3 Connexin 43 (Cx43) expression is differentially regulated in various brain regions of CLN3$^{\Delta ex7/8}$ mice. Total protein extracts were prepared from the somatosensory cortex (S1C), visual cortex (VC), hippocampus (HPC), striatum (STR), and thalamus (TH) of wild type (WT) and CLN3$^{\Delta ex7/8}$ mice (n = 3–4/group), whereupon samples were analyzed by Western blotting for Cx43. Each blot was stripped and re-probed for β-actin to assess uniformity in gel loading. Results are presented as (A) raw data from the S1C and VC and (B) quantitation following β-actin normalization. Significant differences between WT and CLN3$^{\Delta ex7/8}$ tissues are denoted by asterisks (*$p<0.05$; **$p<0.01$).
(TIF)

Figure S4 Glutamine synthetase (GS) expression is reduced in select brain regions of CLN3$^{\Delta ex7/8}$ mice. Total protein extracts were prepared from the somatosensory cortex (S1C), visual cortex (VC), hippocampus (HPC), striatum (STR), and thalamus (TH) of wild type (WT) and CLN3$^{\Delta ex7/8}$ mice (n = 3–4/group), whereupon samples were analyzed by Western blotting for glutamine synthetase (GS). Each blot was stripped and re-probed for β-actin to assess uniformity in gel loading. Results are presented as (A) raw data from the S1C and VC and (B) quantitation following β-actin normalization. Significant differences between WT and CLN3$^{\Delta ex7/8}$ tissues are denoted by asterisks (*$p<0.05$; **$p<0.01$).
(TIF)

Figure S5 Connexin 30 expression in various brain regions of CLN3$^{\Delta ex7/8}$ mice. Total protein extracts were prepared from the somatosensory cortex (S1C), visual cortex (VC), and hippocampus (HPC) of wild type (WT) and CLN3$^{\Delta ex7/8}$ mice (n = 3–4/group), whereupon samples were analyzed by Western blotting for Cx30. Each blot was stripped and re-probed for β-actin to assess uniformity in gel loading. Results are presented as (A) raw data from the S1C and VC and (B) quantitation following β-actin normalization.
(TIF)

Figure S6 GLAST expression in various brain regions of CLN3$^{\Delta ex7/8}$ mice. Total protein extracts were prepared from the somatosensory cortex (S1C), visual cortex (VC), and hippocampus (HPC) of wild type (WT) and CLN3$^{\Delta ex7/8}$ mice (n = 3–4/group), whereupon samples were analyzed by Western blotting for GLAST. Each blot was stripped and re-probed for β-actin to assess uniformity in gel loading. Results are presented as (A) raw data from the S1C and VC and (B) quantitation following β-actin normalization.
(TIF)

Figure S7 *In vivo* administration of INI-0602 does not alter HC activity in CLN3$^{\Delta ex7/8}$ mice. CLN3$^{\Delta ex7/8}$ and wild type (WT) mice were treated with INI-0602 (10 mg/kg) or PBS from postnatal day 30 to 60, whereupon EtBr uptake was measured in CTB stained astrocytes in the somatosensory cortex (S1C), visual cortex (VC), hippocampus (HPC), striatum (STR), and thalamus (TH) as a quantitative measure of HC activity, which is expressed in arbitrary units (a.u.) per min (n = 9 mice/group). Significant differences between WT and CLN3$^{\Delta ex7/8}$ mice are indicated by asterisks (*$p<0.05$, **$p<0.01$, ***$p<0.001$).
(TIF)

Table S1 Electrophysiological parameters of cortical astrocytes in CLN3$^{\Delta ex7/8}$ and WT mice.
(DOCX)

Table S2 Electrophysiological parameters of hippocampal astrocytes in CLN3$^{\Delta ex7/8}$ and wild type (WT) mice.
(DOCX)

Table S3 *In vivo* administration of INI-0602 does not alter blood chemistry profiles in either WT or CLN3$^{\Delta ex7/8}$ mice.
(DOCX)

Acknowledgments

The authors thank Amanda Angle for assistance with mouse breeding colonies and Melissa Mellon in the UNMC Small Animal Imaging Facility for assistance with MR spectroscopy analysis.

Author Contributions

Conceived and designed the experiments: MBurkovetskaya NK TK. Performed the experiments: NK JX MBosch MDB. Analyzed the data: MBurkovetskaya NK MDB TK. Contributed reagents/materials/analysis tools: HT AS. Wrote the paper: MBurkovetskaya NK TK.

References

1. Isolation of a novel gene underlying Batten disease, CLN3. (1995) The International Batten Disease Consortium. Cell 82: 949–957.
2. Wang S (2012) Juvenile neuronal ceroid lipofuscinoses. Adv Exp Med Biol 724: 138–142.
3. Rakheja D, Narayan SB, Bennett MJ (2007) Juvenile neuronal ceroid-lipofuscinosis (Batten disease): a brief review and update. Curr Mol Med 7: 603–608.
4. Staropoli JF, Haliw L, Biswas S, Garrett L, Holter SM, et al. (2012) Large-scale phenotyping of an accurate genetic mouse model of JNCL identifies novel early pathology outside the central nervous system. PLoS One 7: e38310.
5. Tyynela J, Cooper JD, Khan MN, Shemilts SJ, Haltia M (2004) Hippocampal pathology in the human neuronal ceroid-lipofuscinoses: distinct patterns of storage deposition, neurodegeneration and glial activation. Brain Pathol 14: 349–357.
6. Weimer JM, Benedict JW, Getty AL, Pontikis CC, Lim MJ, et al. (2009) Cerebellar defects in a mouse model of juvenile neuronal ceroid lipofuscinosis. Brain Res 1266: 93–107.
7. Anderson GW, Goebel HH, Simonati A (2012) Human pathology in NCL. Biochim Biophys Acta.
8. Pontikis CC, Cotman SL, MacDonald ME, Cooper JD (2005) Thalamocortical neuron loss and localized astrocytosis in the Cln3Deltaex7/8 knock-in mouse model of Batten disease. Neurobiol Dis 20: 823–836.
9. Hagopian K, Lake BD, Winchester BG, Clark JB (1995) Late-infantile Batten disease: purification of the subunit c of the mitochondrial ATP synthase from storage material. Am J Med Genet 57: 272–278.
10. Johnson DW, Speier S, Qian WH, Lane S, Cook A, et al. (1995) Role of subunit-9 of mitochondrial ATP synthase in Batten disease. Am J Med Genet 57: 350–360.
11. Sulzer D, Mosharov E, Talloczy Z, Zucca FA, Simon JD, et al. (2008) Neuronal pigmented autophagic vacuoles: lipofuscin, neuromelanin, and ceroid as macroautophagic responses during aging and disease. J Neurochem 106: 24–36.
12. Riga D, Riga S, Halalau F, Schneider F (2006) Brain lipopigment accumulation in normal and pathological aging. Ann N Y Acad Sci 1067: 158–163.
13. Braak E, Sandmann-Keil D, Rub U, Gai WP, de Vos RA, et al. (2001) alpha-synuclein immunopositive Parkinson's disease-related inclusion bodies in lower brain stem nuclei. Acta Neuropathol 101: 195–201.
14. Seehafer SS, Pearce DA (2006) You say lipofuscin, we say ceroid: defining autofluorescent storage material. Neurobiol Aging 27: 576–588.
15. Aberg L, Liewendahl K, Nikkinen P, Autti T, Rinne JO, et al. (2000) Decreased striatal dopamine transporter density in JNCL patients with parkinsonian symptoms. Neurology 54: 1069–1074.
16. Micsenyi MC, Sikora J, Stephney G, Dobrenis K, Walkley SU (2013) Lysosomal membrane permeability stimulates protein aggregate formation in neurons of a lysosomal disease. J Neurosci 33: 10815–10827.
17. Bras J, Verloes A, Schneider SA, Mole SE, Guerreiro RJ (2012) Mutation of the parkinsonism gene ATP13A2 causes neuronal ceroid-lipofuscinosis. Hum Mol Genet 21: 2646–2650.
18. Kettenmann H, Hanisch UK, Noda M, Verkhratsky A (2011) Physiology of microglia. Physiol Rev 91: 461–553.
19. Rose CF, Verkhratsky A, Parpura V (2013) Astrocyte glutamine synthetase: pivotal in health and disease. Biochem Soc Trans 41: 1518–1524.
20. Pontikis CC, Cella CV, Parihar N, Lim MJ, Chakrabarti S, et al. (2004) Late onset neurodegeneration in the Cln3−/− mouse model of juvenile neuronal ceroid lipofuscinosis is preceded by low level glial activation. Brain Res 1023: 231–242.
21. Xiong J, Kielian T (2013) Microglia in Juvenile Neuronal Ceroid Lipofuscinosis (JNCL) are primed towards a proinflammatory phenotype. J Neurochem.
22. Wallraff A, Kohling R, Heinemann U, Theis M, Willecke K, et al. (2006) The impact of astrocytic gap junctional coupling on potassium buffering in the hippocampus. J Neurosci 26: 5438–5447.
23. Takahashi DK, Vargas JR, Wilcox KS (2010) Increased coupling and altered glutamate transport currents in astrocytes following kainic-acid-induced status epilepticus. Neurobiol Dis 40: 573–585.
24. Rouach N, Koulakoff A, Abudara V, Willecke K, Giaume C (2008) Astroglial metabolic networks sustain hippocampal synaptic transmission. Science 322: 1551–1555.
25. Eugenin EA, Basilio D, Saez JC, Orellana JA, Raine CS, et al. (2012) The role of gap junction channels during physiologic and pathologic conditions of the human central nervous system. J Neuroimmune Pharmacol 7: 499–518.
26. Kielian T (2008) Glial connexins and gap junctions in CNS inflammation and disease. J Neurochem 106: 1000–1016.
27. Scemes E, Spray DC, Meda P (2009) Connexins, pannexins, innexins: novel roles of "hemi-channels". Pflugers Arch 457: 1207–1226.
28. Shestopalov VI, Panchin Y (2008) Pannexins and gap junction protein diversity. Cell Mol Life Sci 65: 376–394.
29. Giaume C, Theis M (2009) Pharmacological and genetic approaches to study connexin-mediated channels in glial cells of the central nervous system. Brain Res Rev.
30. Spray DC, Ye ZC, Ransom BR (2006) Functional connexin "hemichannels": a critical appraisal. Glia 54: 758–773.
31. Bennett MV, Contreras JE, Bukauskas FF, Saez JC (2003) New roles for astrocytes: gap junction hemichannels have something to communicate. Trends Neurosci 26: 610–617.
32. Ransom B, Behar T, Nedergaard M (2003) New roles for astrocytes (stars at last). Trends Neurosci 26: 520–522.
33. Ransom BR (2000) Glial modulation of neural excitability mediated by extracellular pH: a hypothesis revisited. Prog Brain Res 125: 217–228.
34. Anderson CM, Swanson RA (2000) Astrocyte glutamate transport: review of properties, regulation, and physiological functions. Glia 32: 1–14.
35. Haydon PG (2001) GLIA: listening and talking to the synapse. Nat Rev Neurosci 2: 185–193.
36. Volterra A, Meldolesi J (2005) Astrocytes, from brain glue to communication elements: the revolution continues. Nat Rev Neurosci 6: 626–640.
37. Takano T, Tian GF, Peng W, Lou N, Libionka W, et al. (2006) Astrocyte-mediated control of cerebral blood flow. Nat Neurosci 9: 260–267.
38. Mulligan SJ, MacVicar BA (2004) Calcium transients in astrocyte endfeet cause cerebrovascular constrictions. Nature 431: 195–199.
39. Boustany RM (2013) Lysosomal storage diseases–the horizon expands. Nat Rev Neurol 9: 583–598.
40. Mink JW, Augustine EF, Adams HR, Marshall FJ, Kwon JM (2013) Classification and natural history of the neuronal ceroid lipofuscinoses. J Child Neurol 28: 1101–1105.
41. Karpuk N, Burkovetskaya M, Fritz T, Angle A, Kielian T (2011) Neuroinflammation leads to region-dependent alterations in astrocyte gap junction communication and hemichannel activity. J Neurosci 31: 414–425.
42. Orellana JA, Shoji KF, Abudara V, Ezan P, Amigou E, et al. (2011) Amyloid beta-induced death in neurons involves glial and neuronal hemichannels. J Neurosci 31: 4962–4977.
43. Orellana JA, Saez JC, Bennett MV, Berman JW, Morgello S, et al. (2013) HIV increases the release of dickkopf-1 protein from human astrocytes by a Cx43 hemichannel-dependent mechanism. J Neurochem.
44. Groh J, Kuhl TG, Ip CW, Nelvagal HR, Sri S, et al. (2013) Immune cells perturb axons and impair neuronal survival in a mouse model of infantile neuronal ceroid lipofuscinosis. Brain 136: 1083–1101.
45. Qiao X, Lu JY, Hofmann SL (2007) Gene expression profiling in a mouse model of infantile neuronal ceroid lipofuscinosis reveals upregulation of immediate early genes and mediators of the inflammatory response. BMC Neurosci 8: 95.
46. Macauley SL, Pekny M, Sands MS (2011) The role of attenuated astrocyte activation in infantile neuronal ceroid lipofuscinosis. J Neurosci 31: 15575–15585.
47. Jalanko A, Vesa J, Manninen T, von Schantz C, Minye H, et al. (2005) Mice with Ppt1Deltaex4 mutation replicate the INCL phenotype and show an inflammation-associated loss of interneurons. Neurobiol Dis 18: 226–241.
48. Nimmerjahn A, Kirchhoff F, Kerr JN, Helmchen F (2004) Sulforhodamine 101 as a specific marker of astroglia in the neocortex in vivo. Nat Methods 1: 31–37.
49. Tauskela JS, Hewitt K, Kang LP, Comas T, Gendron T, et al. (2000) Evaluation of glutathione-sensitive fluorescent dyes in cortical culture. Glia 30: 329–341.
50. Sebastia J, Cristofol R, Martin M, Rodriguez-Farre E, Sanfeliu C (2003) Evaluation of fluorescent dyes for measuring intracellular glutathione content in primary cultures of human neurons and neuroblastoma SH-SY5Y. Cytometry A 51: 16–25.
51. Dringen R, Hirrlinger J (2003) Glutathione pathways in the brain. Biol Chem 384: 505–516.
52. Cotman SL, Vrbanac V, Lebel LA, Lee RL, Johnson KA, et al. (2002) Cln3(Deltaex7/8) knock-in mice with the common JNCL mutation exhibit progressive neurologic disease that begins before birth. Hum Mol Genet 11: 2709–2721.
53. Kovacs AD, Saje A, Wong A, Ramji S, Cooper JD, et al. (2012) Age-dependent therapeutic effect of memantine in a mouse model of juvenile Batten disease. Neuropharmacology 63: 769–775.
54. Finn R, Kovacs AD, Pearce DA (2011) Altered sensitivity of cerebellar granule cells to glutamate receptor overactivation in the Cln3(Deltaex7/8)-knock-in mouse model of juvenile neuronal ceroid lipofuscinosis. Neurochem Int 58: 648–655.
55. Kovacs AD, Saje A, Wong A, Szenasi G, Kiricsi P, et al. (2011) Temporary inhibition of AMPA receptors induces a prolonged improvement of motor

performance in a mouse model of juvenile Batten disease. Neuropharmacology 60: 405–409.
56. Taylor RM, Farrow BR (1988) Ceroid-lipofuscinosis in border collie dogs. Acta Neuropathol 75: 627–631.
57. Weissenbock H, Rossel C (1997) Neuronal ceroid-lipofuscinosis in a domestic cat: clinical, morphological and immunohistochemical findings. J Comp Pathol 117: 17–24.
58. Oliveira VC, Carrara RC, Simoes DL, Saggioro FP, Carlotti CG, Jr., et al. (2010) Sudan Black B treatment reduces autofluorescence and improves resolution of in situ hybridization specific fluorescent signals of brain sections. Histol Histopathol 25: 1017–1024.
59. Salek RM, Pears MR, Cooper JD, Mitchison HM, Pearce DA, et al. (2011) A metabolomic comparison of mouse models of the Neuronal Ceroid Lipofuscinoses. J Biomol NMR 49: 175–184.
60. Brockmann K, Pouwels PJ, Christen HJ, Frahm J, Hanefeld F (1996) Localized proton magnetic resonance spectroscopy of cerebral metabolic disturbances in children with neuronal ceroid lipofuscinosis. Neuropediatrics 27: 242–248.
61. Pears MR, Cooper JD, Mitchison HM, Mortishire-Smith RJ, Pearce DA, et al. (2005) High resolution 1H NMR-based metabolomics indicates a neurotransmitter cycling deficit in cerebral tissue from a mouse model of Batten disease. J Biol Chem 280: 42508–42514.
62. Eugenin EA, Eckardt D, Theis M, Willecke K, Bennett MV, et al. (2001) Microglia at brain stab wounds express connexin 43 and in vitro form functional gap junctions after treatment with interferon-gamma and tumor necrosis factor-alpha. Proc Natl Acad Sci U S A 98: 4190–4195.
63. Garg S, Md Syed M, Kielian T (2005) Staphylococcus aureus-derived peptidoglycan induces Cx43 expression and functional gap junction intercellular communication in microglia. J Neurochem 95: 475–483.
64. Nagasawa K, Chiba H, Fujita H, Kojima T, Saito T, et al. (2006) Possible involvement of gap junctions in the barrier function of tight junctions of brain and lung endothelial cells. J Cell Physiol 208: 123–132.
65. Moriyama Y, Takagi N, Itokawa C, Tanonaka K (2013) Injection of neural progenitor cells attenuates decrease in level of connexin 43 in brain capillaries after cerebral ischemia. Neurosci Lett 543: 152–156.
66. Li AF, Sato T, Haimovici R, Okamoto T, Roy S (2003) High glucose alters connexin 43 expression and gap junction intercellular communication activity in retinal pericytes. Invest Ophthalmol Vis Sci 44: 5376–5382.
67. Corns LF, Deuchars J, Deuchars SA (2013) GABAergic responses of mammalian ependymal cells in the central canal neurogenic niche of the postnatal spinal cord. Neurosci Lett 553: 57–62.
68. Takeuchi H, Mizoguchi H, Doi Y, Jin S, Noda M, et al. (2011) Blockade of gap junction hemichannel suppresses disease progression in mouse models of amyotrophic lateral sclerosis and Alzheimer's disease. PLoS One 6: e21108.
69. Pautler RG (2004) Mouse MRI: concepts and applications in physiology. Physiology (Bethesda) 19: 168–175.
70. Chatziioannou AF (2005) Instrumentation for molecular imaging in preclinical research: Micro-PET and Micro-SPECT. Proc Am Thorac Soc 2: 533–536, 510–511.
71. Valenzuela MJ, Sachdev P (2001) Magnetic resonance spectroscopy in AD. Neurology 56: 592–598.
72. Kuhl TG, Dihanich S, Wong AM, Cooper JD (2013) Regional brain atrophy in mouse models of neuronal ceroid lipofuscinosis: a new rostrocaudal perspective. J Child Neurol 28: 1117–1122.
73. Orellana JA, Figueroa XF, Sanchez HA, Contreras-Duarte S, Velarde V, et al. (2011) Hemichannels in the Neurovascular Unit and White Matter Under Normal and Inflamed Conditions. CNS Neurol Disord Drug Targets.
74. Tsai G, Coyle JT (1995) N-acetylaspartate in neuropsychiatric disorders. Prog Neurobiol 46: 531–540.
75. Tecedor L, Stein CS, Schultz ML, Farwanah H, Sandhoff K, et al. (2013) CLN3 Loss Disturbs Membrane Microdomain Properties and Protein Transport in Brain Endothelial Cells. J Neurosci 33: 18065–18079.
76. Fossale E, Wolf P, Espinola JA, Lubicz-Nawrocka T, Teed AM, et al. (2004) Membrane trafficking and mitochondrial abnormalities precede subunit c deposition in a cerebellar cell model of juvenile neuronal ceroid lipofuscinosis. BMC Neurosci 5: 57.
77. Wolfe DM, Padilla-Lopez S, Vitiello SP, Pearce DA (2011) pH-dependent localization of Btn1p in the yeast model for Batten disease. Dis Model Mech 4: 120–125.
78. Tovar KR, Maher BJ, Westbrook GL (2009) Direct actions of carbenoxolone on synaptic transmission and neuronal membrane properties. J Neurophysiol 102: 974–978.
79. Bramley JR, Wiles EM, Sollars PJ, Pickard GE (2011) Carbenoxolone blocks the light-evoked rise in intracellular calcium in isolated melanopsin ganglion cell photoreceptors. PLoS One 6: e22721.
80. Rouach N, Segal M, Koulakoff A, Giaume C, Avignone E (2003) Carbenoxolone blockade of neuronal network activity in culture is not mediated by an action on gap junctions. J Physiol 553: 729–745.
81. Bastiaanse EM, Jongsma HJ, van der Laarse A, Takens-Kwak BR (1993) Heptanol-induced decrease in cardiac gap junctional conductance is mediated by a decrease in the fluidity of membranous cholesterol-rich domains. J Membr Biol 136: 135–145.
82. Locke D, Harris AL (2009) Connexin channels and phospholipids: association and modulation. BMC Biol 7: 52.
83. Nagy JI, Lynn BD, Tress O, Willecke K, Rash JE (2011) Connexin26 expression in brain parenchymal cells demonstrated by targeted connexin ablation in transgenic mice. Eur J Neurosci 34: 263–271.
84. Iglesias R, Dahl G, Qiu F, Spray DC, Scemes E (2009) Pannexin 1: the molecular substrate of astrocyte "hemichannels". J Neurosci 29: 7092–7097.
85. Scemes E, Suadicani SO, Dahl G, Spray DC (2007) Connexin and pannexin mediated cell-cell communication. Neuron Glia Biol 3: 199–208.
86. Munroe PB, Mitchison HM, O'Rawe AM, Anderson JW, Boustany RM, et al. (1997) Spectrum of mutations in the Batten disease gene, CLN3. Am J Hum Genet 61: 310–316.
87. Herrmann P, Druckrey-Fiskaaen C, Kouznetsova E, Heinitz K, Bigl M, et al. (2008) Developmental impairments of select neurotransmitter systems in brains of Cln3(Deltaex7/8) knock-in mice, an animal model of juvenile neuronal ceroid lipofuscinosis. J Neurosci Res 86: 1857–1870.
88. Zhuo L, Sun B, Zhang CL, Fine A, Chiu SY, et al. (1997) Live astrocytes visualized by green fluorescent protein in transgenic mice. Dev Biol 187: 36–42.
89. Miyasaka N, Takahashi K, Hetherington HP (2006) Fully automated shim mapping method for spectroscopic imaging of the mouse brain at 9.4 T. Magn Reson Med 55: 198–202.
90. Ratiney H, Coenradie Y, Cavassila S, van Ormondt D, Graveron-Demilly D (2004) Time-domain quantitation of 1H short echo-time signals: background accommodation. MAGMA 16: 284–296.
91. Ratiney H, Sdika M, Coenradie Y, Cavassila S, van Ormondt D, et al. (2005) Time-domain semi-parametric estimation based on a metabolite basis set. NMR Biomed 18: 1–13.
92. Paxinos G, Franklin K.B.J. (2001) The Mouse Brain in Stereotaxic Coordinates. San Diego: Academic Press.
93. Karpuk N, Burkovetskaya M, Kielian T (2012) Neuroinflammation alters voltage-dependent conductance in striatal astrocytes. J Neurophysiol 108: 112–123.
94. Esen N, Shuffield D, Syed MM, Kielian T (2007) Modulation of connexin expression and gap junction communication in astrocytes by the gram-positive bacterium S. aureus. Glia 55: 104–117.

JNI JOURNAL OF NEUROINFLAMMATION

RESEARCH Open Access

FGF-2 released from degenerating neurons exerts microglial-induced neuroprotection via FGFR3-ERK signaling pathway

Mariko Noda[1,2], Kento Takii[1], Bijay Parajuli[1], Jun Kawanokuchi[1], Yoshifumi Sonobe[1], Hideyuki Takeuchi[1], Tetsuya Mizuno[1*] and Akio Suzumura[1]

Abstract

Background: The accumulation of activated microglia is a hallmark of various neurodegenerative diseases. Microglia may have both protective and toxic effects on neurons through the production of various soluble factors, such as chemokines. Indeed, various chemokines mediate the rapid and accurate migration of microglia to lesions. In the zebra fish, another well-known cellular migrating factor is fibroblast growth factor-2 (FGF-2). Although FGF-2 does exist in the mammalian central nervous system (CNS), it is unclear whether FGF-2 influences microglial function.

Methods: The extent of FGF-2 release was determined by ELISA, and the expression of its receptors was examined by immunocytochemistry. The effect of several drug treatments on a neuron and microglia co-culture system was estimated by immunocytochemistry, and the neuronal survival rate was quantified. Microglial phagocytosis was evaluated by immunocytochemistry and quantification, and microglial migration was estimated by fluorescence-activated cell sorting (FACS). Molecular biological analyses, such as Western blotting and promoter assay, were performed to clarify the FGF-2 downstream signaling pathway in microglia.

Results: Fibroblast growth factor-2 is secreted by neurons when damaged by glutamate or oligomeric amyloid β 1-42. FGF-2 enhances microglial migration and phagocytosis of neuronal debris, and is neuroprotective against glutamate toxicity through FGFR3-extracellular signal-regulated kinase (ERK) signaling pathway, which is directly controlled by Wnt signaling in microglia.

Conclusions: FGF-2 secreted from degenerating neurons may act as a 'help-me' signal toward microglia by inducing migration and phagocytosis of unwanted debris.

Keywords: ERK, FGF-2, FGFR3, microglia, neuroprotection, Wnt

Background

Neuron and glial cells are in close association with each other and maintain physiological function in the central nervous system (CNS). When their finely controlled interactions are impaired by inflammation and stress conditions, neuronal networks are damaged, which results in the pathogenesis of several neurodegenerative diseases [1-3]. It has been proposed that apoptotic cells or degenerating neurons release various signals to surrounding glial cells. These signals have been recently classified as 'find-me', 'help-me', and 'eat-me' signals [4-8].

Microglia are resident immune cells in the CNS and express many versatile receptors [9]. Therefore, they are considered the main recipient of various signals from degenerating neurons. Moreover, microglia exhibit early and rapid responses to various stimuli; for instance, activated microglia accumulate at pathological lesions [10]. The rapid and accurate migration of microglia to lesions is predominantly mediated by various chemokines [11]. In addition to chemokines, fibroblast growth factor (FGF)-2 regulates cellular migration in developing brain and in zebra fish [12-15]; however, FGF-2 has not been directly implicated in microglial migration.

* Correspondence: tmizuno@riem.nagoya-u.ac.jp
[1]Department of Neuroimmunology, Research Institute of Environmental Medicine, Nagoya University, Furo-cho, Chikusa-ku, Nagoya 464-8601, Japan
Full list of author information is available at the end of the article

Fibroblast growth factor, purified from pituitary extracts, has a variety of functions, including inducing the proliferation and differentiation of various cell types, such as fibroblasts. Twenty-two types of FGF have been identified in human beings, as well as in mice. FGF-2 (basic FGF), one of the most common FGFs, has attracted attention for its widespread activity, such as cell proliferation, carcinoma cell invasion, neoangiogenesis, osteogenesis, and differentiation of developmentally staged constituent cells of the CNS [16-19]. FGF-2 is expressed in various tissues at low levels, but its concentration is much higher in the brain. Five types of FGF receptor (FGFR: FGFR1 to 5) have been identified to date [20], but their detailed expression levels in individual cells and mode of action in the CNS have not been elucidated. However, the expression levels of FGF-2 and FGFR have been shown to be up-regulated in CNS injury [21]. Furthermore, several reports show that astrocytes, but not neuronal cells, are the dominant FGF-2-producing cells in the CNS [16-19].

FGF-2 plays important roles in various cells in the CNS. Indeed, morphological change in glial cells and reactivity *in vivo* [22] have been demonstrated with FGF-2 injection into the cerebrospinal fluid. The best known FGF receptor–related signaling is MAPK, which is the common downstream signaling pathway of all FGFR subtypes. FGF-2 is known to induce Wnt/β-catenin signaling in human endothelial cells and developing the zebra fish brain [12,23,24], but it is unclear whether FGF-2 also regulates Wnt/β-catenin signaling in microglia under neurodegenerative conditions.

In this study, we found that FGF-2 was secreted by glutamate or oligomeric amyloid β (oAβ) from damaged neurons, but not from astrocytes or microglia. Degenerating neurons produce signaling molecules that attract surrounding cells including microglia. Among these signaling molecules, we revealed FGF-2 as a predominant coordinator of microglial migration. FGF-2 induced microglial neuroprotection, migration and phagocytosis of neuronal debris via FGFR3. Furthermore, downstream signaling of FGF-2, especially through the FGFR3-extracellular signal-regulated kinase (ERK) signaling pathway, led to microglia-mediated neuronal survival. Wnt signaling directly induced this ERK phosphorylation and microglial migration, which were each enhanced by FGF-2 stimulation. Together, our results demonstrate that FGF-2 could be a key signaling molecule for crosstalk between degenerating neurons and microglia, and that the FGFR3/ERK/Wnt signaling pathway contributes to the induction of microglial neuroprotection.

Methods

Reagents

L-glutamate and goat immunoglobulin G (IgG), mouse IgG, and rat IgG were purchased from Sigma (St. Louis, MO, USA). Mouse recombinant FGF-2, mouse recombinant fractalkine (FKN; the chemokine domain), CCL21, and the FGFR (FGFR2-5) neutralizing antibodies were obtained from R & D Systems (Minneapolis, MN, USA). The MAPK inhibitors (U0126 (MEK1/2 inhibitor), SB203580 (p38 inhibitor), and SP600125 (JNK inhibitor)), PI3K inhibitor wortmannin, FGFR antagonist (PD173074 (pan-FGFR blocker), SU11652 (selective FGFR1 blocker)), and IWR-1-endo (Wnt antagonist) were purchased from Calbiochem (Gibbstown, NJ, USA). FGF-2 neutralizing antibody (aFGF-2) was purchased from Millipore (Billerica, MA, USA), and FKN neutralizing antibody (aFKN) was purchased as previously described [25].

Preparation of Aβ solutions

Aβ1-42 solution was prepared as previously described [26]. Briefly, synthetic human Aβ1-42 (Peptide Institute, Osaka, Japan) was dissolved to 1 mM in 100% 1,1,1,3,3,3-hexafluoro-2-propanol (HFIP). The HFIP was dried and resuspended to a concentration of 5 mM in DMSO. To form oligomers, amyloid peptide was diluted to a final concentration of 100 μM with Ham's F-12, incubated at 4°C for 24 h, and then immediately added to cultures at a final concentration of 5 μM.

Cell culture

The protocols for animal experiments were approved by the Animal Experiment Committee of Nagoya University. Primary neuronal cultures were prepared from the cortices of C57BL/6 mice embryos at embryonic day 17 (E17) as described previously [27]. Briefly, cortical fragments were dissociated into single cells in dissociation solution (Sumitomo Bakelite, Akita, Japan), and resuspended in nerve culture medium (Sumitomo Bakelite). Neurons were seeded onto 12 mm polyethylenimine-coated glass coverslips (Asahi Techno Glass Corp., Chiba, Japan). The purity of the cultures was greater than 95%, as determined by NeuN-specific immunostaining [28].

Microglia were isolated from primary mixed glial cell cultures prepared from newborn C57BL/6 mice at day *in vitro* (DIV) 14 using the 'shaking off' method, which has been described previously [29]. The purity of the cultures was 97 to 100% as determined by immunostaining for the Fc receptor. Cultures were maintained in DMEM supplemented with 10% fetal calf serum, 5 μg/ml bovine insulin, and 0.2% glucose. Astrocytes were purified from primary mixed glial cultures by three or four repetitions of trypsinization and replating. The purity of astrocytes was greater than 95%, as determined by GFAP-specific immunostaining [30].

Measurement of FGF-2 levels

Secreted FGF-2 from mouse primary astrocytes, cortical neurons, and microglia were measured using an ELISA

kit (RayBiotech, Inc., Norcross, GA, USA). Neurons were treated with L-glutamate (20 μM) or oAβ (5 μM) for 6 to 24 h at 37°C. Supernatants were then collected and assessed for FGF-2 levels.

Western blotting

Microglial cell lysates were boiled after the addition of sample buffer (1 M Tris-HCl, 20% sodium dodecyl sulfate (SDS), and 2.5% glycerol). Fifty micrograms of total protein were separated on a 5 to 20% Tris-glycine SDS-polyacrylamide gel and blotted onto Hybond-P polyvinylidene difluoride (PVDF) membranes (GE Healthcare UK, Buckinghamshire, UK). Membranes were blocked with 1% skim milk in Tris-buffered saline containing 0.05% Tween 20 for 1 h at room temperature. Primary antibodies to detect phosphorylated and total MAPK (Cell Signaling, Danvers, MA, USA) were applied at the concentrations recommended by the manufacturers. The secondary antibody was horseradish peroxidase-conjugated anti-rabbit IgG (GE Healthcare), which was used at a dilution of 1:1000. SuperSignal West Pico Chemiluminescent Substrate (Thermo Fisher Scientific, Rockford, IL, USA) was used according to the manufacturer's instructions. The intensities of the bands were calculated using the CS Analyzer 1.0 (Atto Corporation, Tokyo, Japan).

Wnt promoter assay

HEK293T cells were seeded one day before transfection by FuGENE HD (Promega, Madison, WI, USA) with a luciferase reporter vector from the Cignal TCF/LEF Reporter (luc) kit (Wnt promoter assay system), which was purchased from SABiosciences (Qiagen KK, Tokyo, Japan). After drug treatment, cells were lysed and luciferase reporter activity was measured using the Dual luciferase reporter assay kit (Promega) and a Wallac 1420 ARVOMX (PerkinElmer Japan, Yokohama, Japan).

Evaluation of microglial phagocytosis

A microglial phagocytosis assay was performed as previously described [25]. Briefly, primary mouse cortical neurons in 24-well plates were labeled on DIV 14 with 1 μM CM-DiI (Molecular Probes), and treated with 20 μM glutamate overnight at 37°C. After changing the culture medium, microglia were added to these neuronal cultures (1:2 ratio for neurons to microglia) with or without FGF-2 for 24 h. Cells were subsequently fixed in 4% paraformaldehyde. Microglia were stained with Cy5-conjugated rat anti-mouse CD11b monoclonal antibodies prior to fixation. Phagocytic uptake of neuronal debris by microglia was estimated based on the detection of DiI-stained neuronal debris [31] in CD11b-positive microglia (green); the phagocytosis index was calculated as the percentage of red staining that overlapped with green staining (shown in yellow) among all of the microglia.

Immunocytochemistry

Cells were fixed with 4% paraformaldehyde, blocked, and permeabilized. Neurons were stained with mouse polyclonal anti–MAP-2 antibody (1:1000; Chemicon, Temecula, CA, USA) and secondary antibody conjugated to Alexa 488 (1:1000; Invitrogen). Astrocytes were stained with mouse monoclonal anti-GFAP antibody (Sigma) and secondary antibody conjugated to Alexa 647 (1:1000; Invitrogen). Microglia were stained with Cy5-conjugated rat anti-mouse CD11b monoclonal antibody (1:300, BD Pharmingen) prior to fixation. Images were analyzed using a deconvolution fluorescence microscope system (BZ-8000; Keyence Corporation, Osaka, Japan). The other primary antibodies included FGFRs, which were purchased from R & D systems and used according to the manufacturer's instructions.

Surviving neurons were identified based on their cytoskeletons as previously described [28]. Viable neurons were strongly stained with anti-MAP-2 antibodies, whereas damaged neurons showed weaker staining. MAP-2-positive neurons were counted in representative areas in each well. Using five independent trials, more than 200 neurons were evaluated in each well by a scorer who was blind to the experimental conditions. The number of viable neurons in untreated cultures was set as 100%.

Measurement of CCL3 (MIP-1a), NO, and glutamate levels

Supernatants from microglia were assessed using the chemokine (C-C motif) ligand 3 (CCL3) ELISA kit (R & D Systems), and a Griess reaction for nitric oxide (NO) detection. To measure glutamate levels, a colorimetric assay kit (Yamasa Corporation, Tokyo, Japan) was used, as previously described [25].

MTS assay

To evaluate the viability of the cells, we used the CellTiter 96 Aqueous One Solution Cell Proliferation Assay kit (Promega) and followed the manufacturer's instructions.

Microglial migration assay

Microglial migration was performed using Transwell plates with 3 μm pore polyethylene terephthalate (PET) membrane filters (BD Biosciences). We placed 800 μl of neuronal-conditioned medium or microglial culture medium treated with drugs into the lower chamber of the Transwell plate. Membrane filters were then put in vacant wells, and 200 μl of microglia-containing medium (1.0×10^5 cells/well) was carefully added on top of the filter membrane to avoid bubbles. These plates were incubated for 24 h. Cells that migrated into the lower wells were counted by fluorescence-activated cell sorting (FACS). Chemokine-treated T cells (combination of FKN

and CCL21 (100 nM each)) were used as positive controls for this method, as previously described [32].

RT-PCR

Total RNA was extracted from astrocytes, microglia, and neurons using an RNeasy Mini Kit (Qiagen, Tokyo, Japan). A first-strand cDNA library was obtained using SuperScript II (Invitrogen, Carlsbad, CA) and oligo (dT) 12-18 (Invitrogen) as the first-strand primer. Negative control reactions were performed using the same system after heat denaturation of reverse transcriptase. RT-PCR was used to amplify transcripts encoding mouse FGF-2, each receptor subtypes and glyceraldehydes-3-phosphate dehydrogenase (GAPDH), using 0.1 μg of first-strand cDNA, Blend Taq polymerase (Toyobo Co., Osaka, Japan), and oligonucleotide primers (Table 1; except for previously described primers for GAPDH [25]).

Statistical analysis

Statistically significant differences between experimental groups were determined by one-way analysis of variance (ANOVA) followed by Dunnett's or Tukey's tests for multiple comparisons. Statistical analysis was performed using the software program Prism 4 for Windows (GraphPad Software, San Diego, CA, USA). *P* values less than 0.05 were considered significant.

Results

Expression of FGFRs in primary neurons and glial cells

We first examined the expression of FGFRs in the CNS. According to our immunocytochemical (Figure 1A) and RT-PCR (Figure 1B) data, all FGF receptors (FGFR1 to 5) were expressed in astrocytes. FGFR1 to 4 were expressed in neurons and microglia. The expression of FGF-2 mRNA was detected in neurons and astrocytes.

Table 1 Oligonucleotide primers used in RT-PCR

Gene	Sequence (5′ to 3′)	Expected size (bp)
FGF-2 sense	5′-AGCGGCTCTACTGCAAGAAC	371
antisense	5′-AGCAGACATTGGAAGAAACAGT	
FGFR1 sense	5′-GTTGGGCTCTGTCATCATCTAT	522
antisense	5′-GCGTACTCCACAATGACATAAA	
FGFR2 (IIIb, IIIc) sense	5′-CTCATCCTGCTGGGTCTGAG	748
antisense	5′-AGGAGTAGCAGCTGATGTGAC	
FGFR3 sense	5′-CCTGTGTAGTTGAGAACAAGTTT	625
antisense	5′-GTGTTGGAGTTCATAGAGGAGT	
FGFR4 sense	5′-GAGGTCTTGTATCTGAGGAACG	651
antisense	5′-GTTCTTGTGTCTTCCGATTAGC	
FGFR5 sense	5′-ATGATATTAGTCCAGGGAAGG	366
antisense	5′-GGATTACATCCACTTTGTAGGT	

Glutamate or oAβ enhances FGF-2 release from neurons, and FGF-2 induces microglial neuroprotection via FGFR3

FGF-2 is widely expressed in the CNS, especially in astrocytes, while FGF-5, FGF-8, and FGF-9 are synthesized by neurons [33]. FGF-2 is reported to be produced by cerebellar granule neurons in co-cultures with microglia, and to abrogate quinolinic acid–mediated neurotoxicity [31]. In this study, we investigated whether cortical neurons could produce FGF-2 in response to neurotoxic stimuli. We found that treatment for 6 h and 24 h with 20 μM glutamate or 5 μM oAβ significantly induced FGF-2 release from cortical neurons (Figure 2A). Astrocytes typically secrete FGF-2; however, various stimuli including glutamate, oAβ, lipopolysaccharide (LPS), and other proinflammatory cytokines did not enhance FGF-2 secretion by astrocytes (Figure 2B). Furthermore, FGF-2 secretion by microglia was barely detectable (Figure 2B).

Next, we determined whether FGF-2 might exert microglial neuroprotection. As shown in Figure 3A,B, treatment with 20 μM glutamate induced apparent neuronal cell death in neuron-microglia co-cultures. The addition of 100 ng/ml FGF-2 significantly ameliorated neurotoxicity, while an anti-FGF-2 antibody canceled the effect. The addition of rat IgG (isotype-matched control for anti-FGF-2 antibody) had no effect on cell survival rate. In neuronal cultures, neuronal cell death was not ameliorated by FGF-2 treatment. There seems to be little difference in neuronal survival against Glu-induced excitotoxicity with or without microglia. We considered that the secreted level of FGF-2 from Glu-treated neurons might not reach the effective dose to enhance the neuronal survival. In addition, FGF-2 treatment suppressed the proinflammatory response of activated microglia through the inhibition of neurotoxic molecules, such as glutamate and NO (Additional file 1: Figure S1A,B). FGF-2 had no effect on microglial proliferation (Additional file 1: Figure S1C). FGF-2 dose-dependently enhanced the neuronal survival in the presence of microglia (Additional file 1: Figure S2).

To investigate the underlying mechanism of neuroprotection by FGF-2 in microglia, we used FGFR inhibitors and neutralizing antibodies. The neuroprotective effect of 100 ng/ml FGF-2 was completely canceled by treatment with pan-FGFR inhibitor PD173074, or anti-FGFR3 neutralizing antibody. Conversely, neutralizing antibodies for FGFR1, 2, 4, and 5, selective FGFR1 blocker SU11652, and isotype control of neutralizing antibodies had no effect on neuronal survival (Figure 3C,D).

CCL3 (MIP-1α) is reported to be a downstream target of FGF-2-induced FGFR3 signaling [34]. FGF-1-induced FGFR3 targets include the Na^+ channel, type III intermediate filament peripherin, and cell surface glycoprotein Thy1 [34,35]. We confirmed that FGF-2 leads to the induction of CCL3 expression in microglia. Using ELISA, CCL3 expression was increased by FGF-2 in a dose-

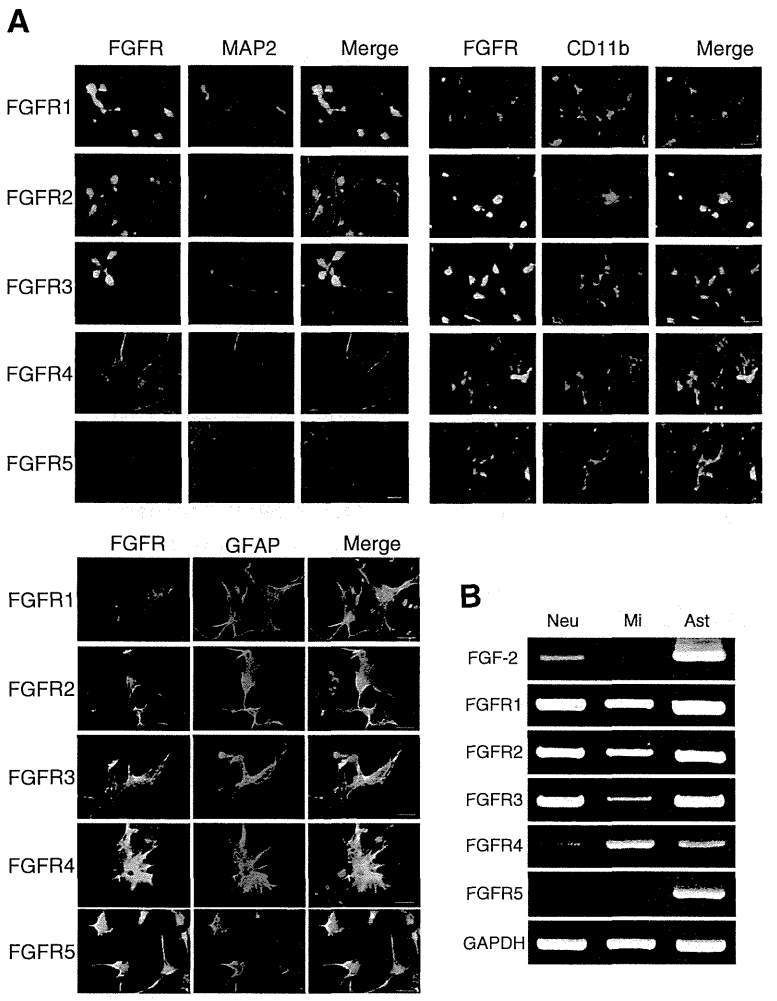

Figure 1 Expression of FGF-2 and FGFRs in primary neurons and glial cells. (A) Expression of FGFRs as assessed by immunocytochemistry: FGFRs (green), MAP-2 (mature cortical neurons; red), CD11b (microglia; red), and GFAP (astrocytes; red). Scale bars, 10 μm in neurons and microglia, and 50 μm in astrocytes. **(B)** Expression of FGF-2 and FGFR1 to FGFR5 mRNA in mature cortical neurons (Neu), microglia (Mi) and astrocytes (Ast), as assessed by RT-PCR. GAPDH expression is used as a control.

dependent manner (Additional file 1: Figure S3). While CCL3 is known as a proinflammatory chemokine, FGF-2 did not activate microglia in this study.

FGF-2-induced microglial neuroprotection via ERK MAPK and ERK activation is directly regulated by Wnt signaling

To elucidate the signaling pathway of microglia-mediated neuroprotection, we examined the effect of several kinase inhibitors on neuronal survival. MAPKs (ERK, p38, and JNK) and phosphoinositide-3 kinase (PI3K) are known as common downstream signaling pathways of FGFRs. We found that inhibition of ERK by U0126 significantly suppressed FGF-2-induced microglial neuroprotection. Other kinase inhibitors (p38, JNK, MAPK, and PI3K inhibitors) did not affect neuroprotection (Figure 4A,B). U0126 might affect both microglia and neurons in the co-culture model. The effects of this signaling on neurons cannot be denied. As shown in Figure 4C, FGF-2 increased ERK phosphorylation in microglia, which peaked within 15 min.

In developmental morphogenic stages and angiogenesis, the coordinated action of Wnt/β-catenin and FGF signaling has been reported [23,24,36]. It has also been reported that mouse primary microglia express the Wnt receptors Frizzled and LDL-related protein 5/6 [37]. Therefore, to clarify the interaction of Wnt signaling with FGF in microglia, we examined the effect of Wnt inhibitor on ERK phosphorylation by FGF-2. Pre-treatment of Wnt antagonist IWR-1-endo showed remarkable inhibition of ERK activation (Figure 4D). FGF-2 also directly increased TCF/LEF promoter activity, which is the downstream target of the Wnt signaling pathway. The FGF-2-induced TCF/LEF promoter activity was completely abrogated by treatment of U0126 or IWR-1-endo (Figure 4E).

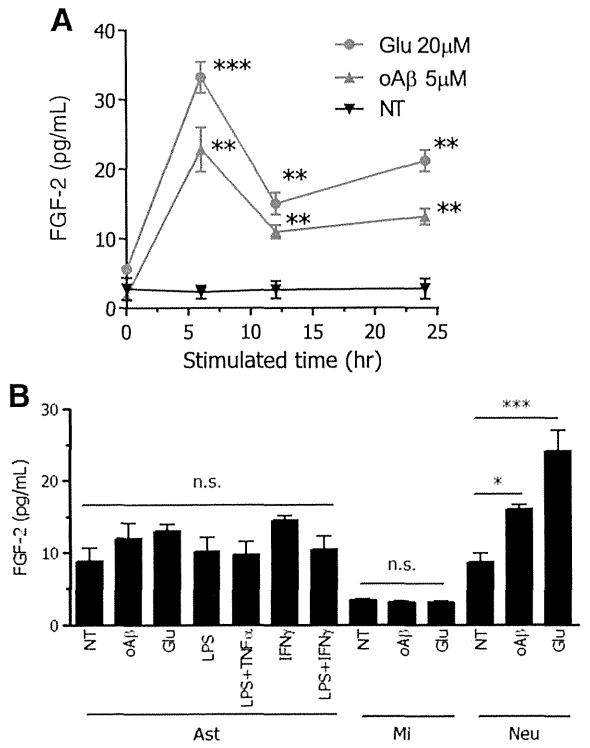

Figure 2 The detection of FGF-2 in primary neurons and glial cells. **(A)** Neurons were treated with glutamate (Glu) or oligomeric amyloid β1-42 (oAβ) at the indicated concentrations. FGF-2 concentrations in the neuronal culture supernatants were measured using ELISAs at each time point. Results show the means with SEM ($n = 3$). Significant differences compared with untreated samples. *: $P < 0.05$, **: $P < 0.01$ (one-way ANOVA with Dunnett's *post-hoc* test). **(B)** Astrocytes, microglia and neurons were treated with Glu (20 μM) or oAβ (5 μM) for 6 h. Other treatments of astrocytes (6 h) were LPS (1 μg/ml), TNF-α (20 ng/ml), IFN-γ (10 ng/ml), and a combination of all three. ELISA was then performed to detect FGF-2 concentration in the culture supernatants. The results show the means with SEM ($n = 3$). Significant differences compared with untreated samples in each cell type. *: $P < 0.05$, ***: $P < 0.001$, n.s.: not significant (one-way ANOVA with Dunnett's *post-hoc* test).

FGF-2 increased microglial migration and clearance of neuronal debris via FGFR3 and Wnt pathway signaling

We next examined the effect of FGF-2 on microglial migration and phagocytosis activity. We established a microglial migration assay, and assessed migration via the Transwell cell culture system. Microglial migration was significantly increased by CCL21, CCL21 plus FKN, and FGF-2 (Additional file 1: Figure S4). We also confirmed the availability of this system in our previous report [32]. T cells from mouse lymph node showed drastic migration by CCL21 plus FKN (Additional file 1: Figure S4B). Neuronal-conditioned media treated with 20 μM glutamate for 24 h can significantly attract microglia (Additional file 1: Figure S4C). As shown in Figure 5A, while fresh neuronal media did not induce microglial migration, untreated neuronal-conditioned media significantly enhanced migration. Furthermore, it has been determined that neuronal-conditional media treated with 20 μM glutamate for 24 h is a more potent attractant to microglia. This effect was canceled by aFGF-2, but not aFKN (Figure 5A). We also revealed that addition of 100 ng/ml FGF-2 to the lower part of the Transwell system significantly enhanced microglial migration (Figure 5B). The effect was canceled by pan-FGFR inhibitor PD173074 and aFGFR3 neutralizing antibody.

Wnt signaling maintains cell migration in the developmental stages. Therefore we next examined whether Wnt signaling could also mediate microglial migration. Wnt antagonist IWR-1-endo dose-dependently attenuated the induction of microglial migration by FGF-2 (Figure 5C). By contrast, ERK MAPK pathway was not directly concerned with microglial migration (Additional file 1: Figure S4D). Furthermore, FGF-2 enhanced microglial phagocytosis of neuronal debris induced by glutamate toxicity (Figure 5D,E). We examined which type of FGFR is involved in the FGF-2-induced phagocytosis, and found that pan-FGFR inhibitor PD173074 and anti-FGFR3 neutralizing antibody suppressed microglial phagocytosis of neuronal debris (Figure 5D,E).

Discussion

Our results indicate that FGF-2 is released from degenerating neurons and induces microglial migration and neuroprotection, which are mediated through the FGFR3-Wnt-ERK signaling pathway. Neurons were fine responders of glutamate and oAβ, and then allowed the release of FGF-2 in relatively short times. FGF receptors are expressed in neurons and glial cells. FGFR3, in particular, is activated by FGF-2 via the ERK MAPK-dependent signaling pathway in microglia. The other FGF, FGF-19, is reported to negatively regulate NFκB via FGFR4 [38]. In the developmental morphogenic stages and angiogenesis, coordinated action of Wnt/β-catenin and FGF signaling has been reported [12,23,24,39]. Recently, expression of Wnt receptors Frizzled and LDL receptor-related protein 5/6 has been reported in mouse primary microglia [37]. In this study, we revealed that FGF-2 directly controlled the Wnt signaling pathway in mouse primary microglia, and that Wnt signaling could also directly regulate microglial migration induced by FGF-2. FGF-2 and the extracellular matrix protein Anosmin-1 have dynamic roles in cellular proliferation and migration from the subventricular zone in CNS development [40]. FGF-2 enhances the proliferation and differentiation of neuronal stem cells. Anosmin-1 and FGF-2 could possibly be diagnostic markers in multiple sclerosis (MS), because their expression level varies between different types of MS [16]. In experimental autoimmune encephalomyelitis, the animal model of MS, FGF-2 may act as a remyelinating and nerve fiber preserving agent [41]. Therefore, FGF-2/Wnt signaling has

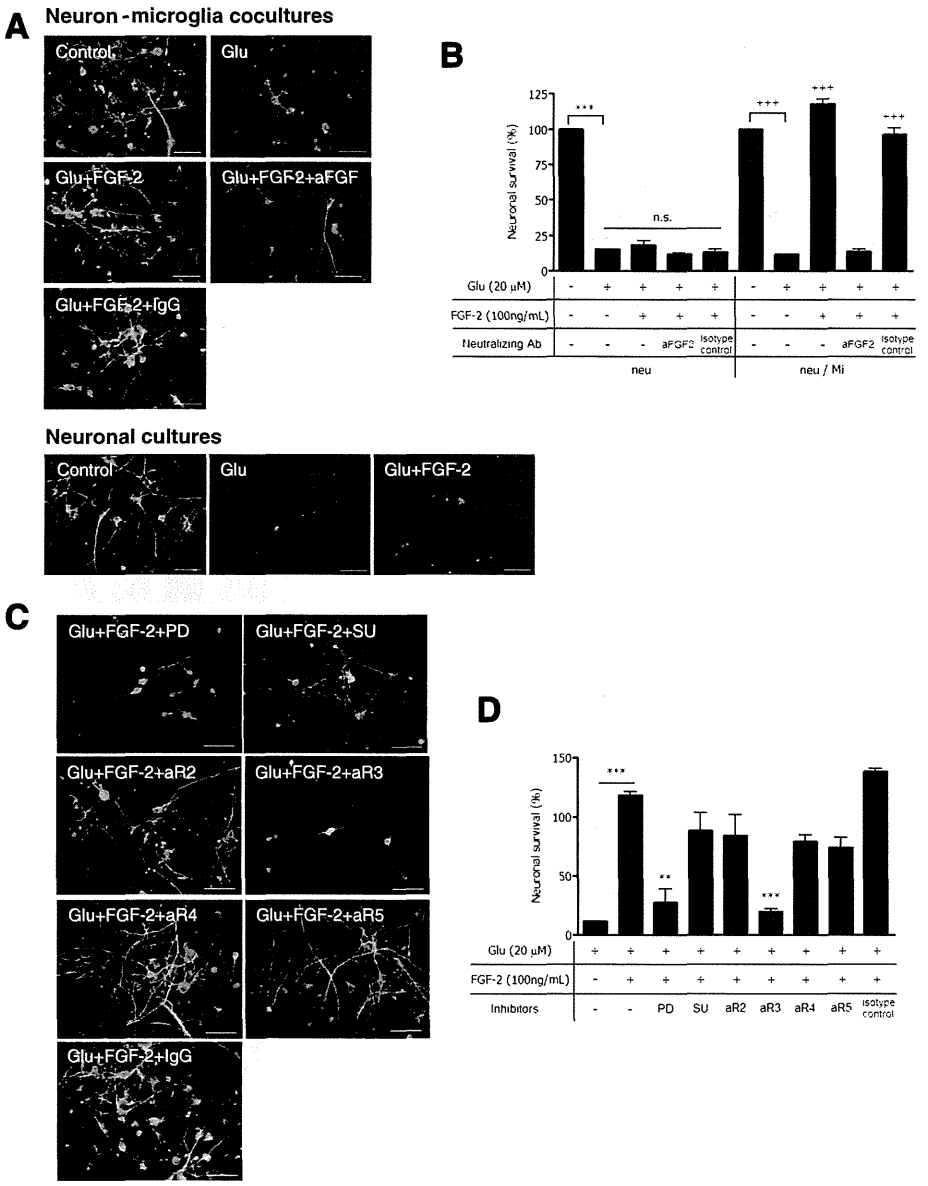

Figure 3 The neuroprotective effects of FGF-2 in neuron-microglia co-cultures. (A) Neuronal cultures were also treated with Glu and FGF-2. Neurons were stained with anti-MAP-2 antibody (green), and microglia were stained with a Cy5-conjugated anti-CD11b antibody (red). Scale bars, 50 μm. **(B)** The neuronal survival rate was calculated as the percentage of intact neurons in the treated sample relative to the untreated sample. The columns indicate mean with SEM from three independent experiments. * indicates significant differences compared with untreated neuronal cultures (***: $P < 0.001$); + indicates significant differences compared with untreated neuron–microglia co-cultures (+++: $P < 0.001$) by one-way ANOVA with Tukey's *post-hoc* test. **(C)** After treatment with 20 μM Glu and 100 ng/ml FGF-2, the inhibitory effects of FGFR were evaluated using FGFR blockers or each anti-FGFR neutralizing antibody (PD, pan-FGFR blocker, 1 μM PD173074; SU, selective FGFR1 blocker, 500 nM SU11652; aR2, anti-FGFR2 antibody; aR3, anti-FGFR3 antibody; aR4, anti-FGFR4 antibody; aR5, anti-FGFR5 antibody; or isotype-matched IgG control). **(D)** The neuronal survival rate was calculated. The columns indicate the means with SEM from three independent experiments, each of which included the analysis of ten randomly selected fields. Significant differences compared with FGF-2-treatment were noted. **: $P < 0.01$, ***: $P < 0.001$ (one-way ANOVA with Tukey's *post-hoc* test).

a potential to regulate cellular proliferation and migration to maintain adult CNS function.

Localized delivery of FGF-2 and brain-derived neurotrophic factor (BDNF) to the lesioned hippocampus increases neurogenesis and reduces epileptogenesis in a rat model of epilepsy [42]. The overexpression of FGF-2/BDNF also attenuates neuroinflammation through suppression of IL-1β [43]. Moreover, FGF-2 gene delivery restores hippocampal functions in an Alzheimer's disease mouse model [44]. FGF-2 has a deep connection

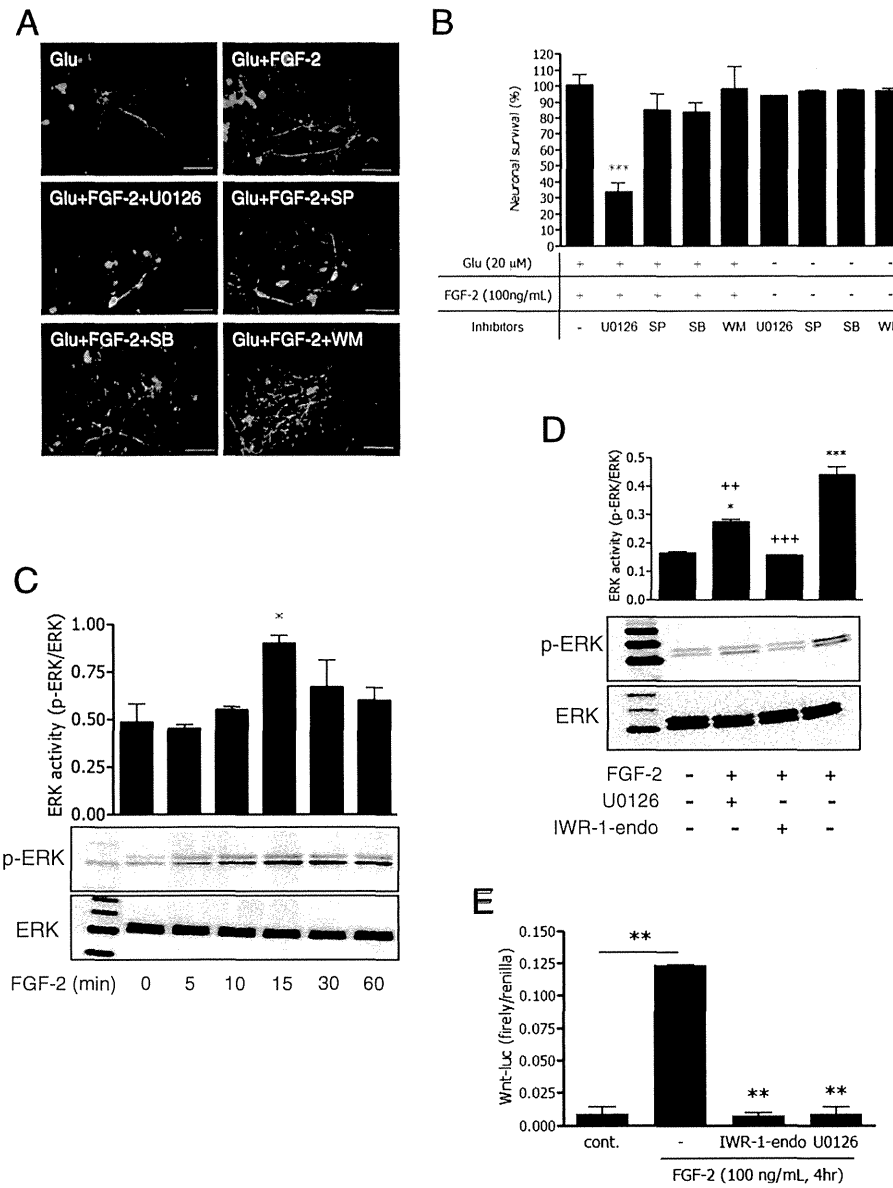

Figure 4 FGF-2 exhibits neuroprotection via ERK MAPK signaling pathway. (A) Effects of MAPK and PI3K inhibitors on neuroprotection of FGF-2. U0126, MEK1/2 inhibitor U0126 (1 μM); SP, JNK inhibitor SP600125 (10 μM); SB, p38 inhibitor SB203580 (10 μM); WM, PI3K inhibitor wortmannin (2 μM). **(B)** Neuronal survival rate. Columns indicate mean with SEM from three independent experiments. ***: $P < 0.001$ compared with the cultures without inhibitors (one-way ANOVA with Dunnett's *post-hoc* test). **(C)** Protein extracts from primary microglia were analyzed by immunoblotting with antibodies specific for phosphorylated and total ERK (ERK1/2). Cells were treated with 100 ng/ml FGF-2 for the indicated periods. *: $P < 0.05$ compared with untreated control (0 min) samples (one-way ANOVA with Dunnett's *post-hoc* test). **(D)** Microglia were treated with U0126 (1 μM) or Wnt antagonist IWR-1-endo (300 nM) overnight and then 100 ng/ml FGF-2 for 15 min. Western blotting of phosphorylated and total ERK was performed. * indicates significant differences compared with untreated samples (*: $P < 0.05$, ***: $P < 0.001$); + indicates significant differences compared with FGF-2 treatment alone (+++: $P < 0.001$) by one-way ANOVA with Tukey's *post-hoc* test. **(E)** Wnt promoter assay. HEK293T cells were transfected with Wnt promoter bearing the firefly luciferase reporter vector and Renilla luciferase reporter vector as a transfection control. After 24 h incubation, cells were treated with IWR-1-endo and U0126 overnight, and then treated with FGF-2 for 4 h. Cells were lysed and measured for luciferase activity. **: $P < 0.01$ compared with FGF-2 treatment alone (one-way ANOVA with Dunnett's *post-hoc* test).

with tumorigenicity. CD44-mediated migration of human inflammatory macrophages into the extravascular compartment depends on binding of FGF-2 to the CD44 receptor [45]. Therefore, it is possible that FGF-2 has functional association with a new counterpart other than FGFRs.

The brain concentration of FGF2 is reported to be around 30 to 120 ng/mg [46]; however, some reports

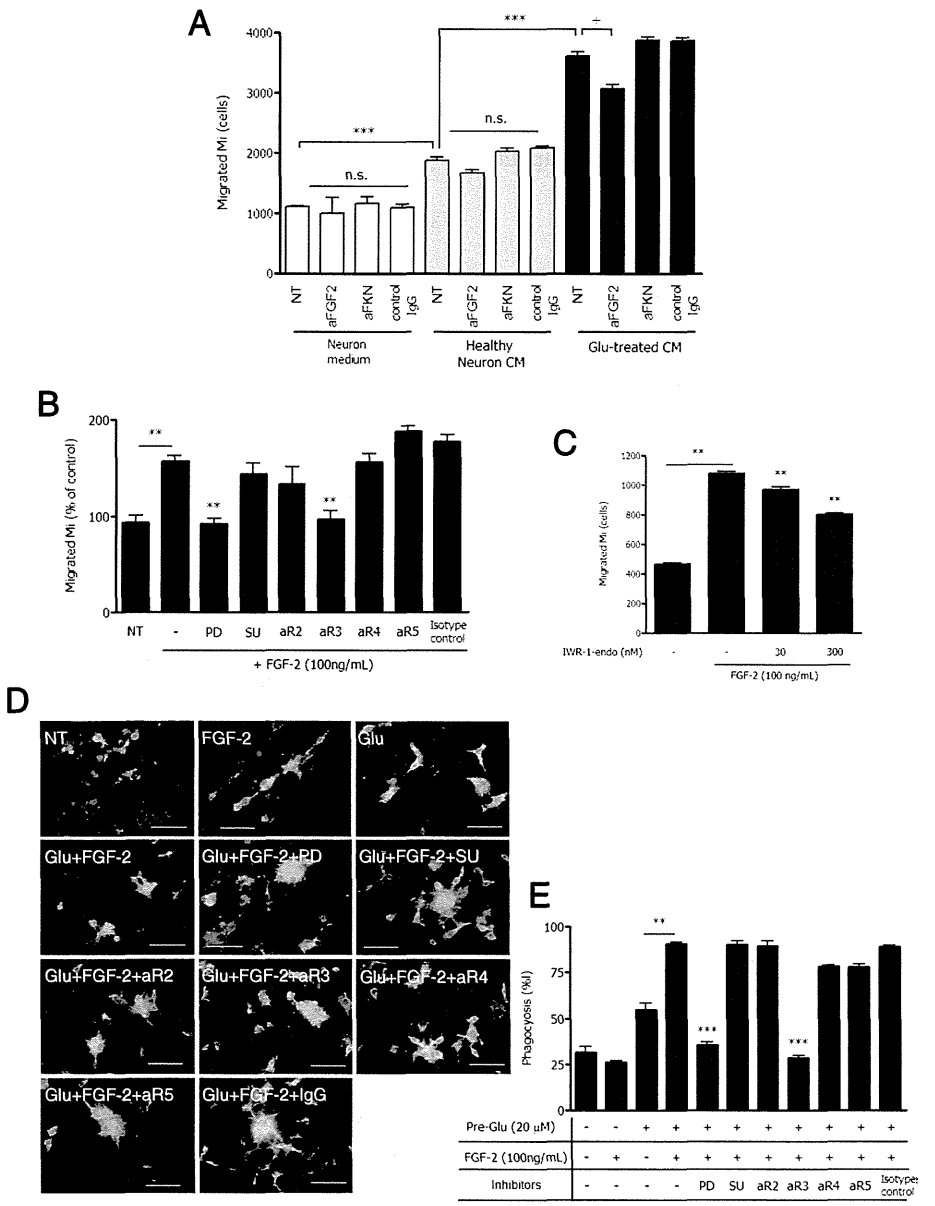

Figure 5 Effects of FGF-2 on cellular migration and clearance of degenerated neuronal debris by microglia. (A) Microglial migration assay; aFKN or aFGF-2 were added to lower plates and microglia set on upper Transwell inserts and cultured for 48 h, with isotype-matched IgG as control. Migrated cells in lower plates were counted by FACS. One-way ANOVA with Tukey's *post-hoc* test: *, significant difference compared with untreated samples using healthy conditioned medium (***: $P < 0.001$); +, significant difference compared with untreated samples (n.s., not significant; +, $P < 0.05$). **(B)** Effect of FGFR blockers and antibodies on microglial migration induced by 100 ng/ml FGF-2. PD, pan-FGFR blocker 1 μM PD173074; SU, selective FGFR1 blocker 500 nM SU11652; aR2, anti-FGFR2 antibody; aR3, anti-FGFR3 antibody; aR4, anti-FGFR4 antibody; aR5, anti-FGFR5 antibody; isotype-matched IgG control. **, $P < 0.01$ compared with FGF-2 treatment alone (one-way ANOVA with Dunnett's *post-hoc* test). **(C)** Effect of IWR-1-endo on microglial migration induced by FGF-2 treatment. **, $P < 0.01$ compared with FGF-2 treatment alone (one-way ANOVA with Dunnett's *post-hoc* test). **(D)** Microglial phagocytosis assay. CM-DiI-labeled neurons were treated with or without glutamate, and microglia were added to the culture. These cells were treated with or without 100 ng/ml FGF-2 and with FGFR blockers or each of the anti-FGFR neutralizing antibodies of (B) for 24 h. Scale bars, 20 μm. **(E)** Phagocytosis index, defined as the percentage of total microglia staining (green) overlapping with DiI staining (red). Columns indicate mean with SEM from three independent experiments. Significant differences compared with sample used degenerated neuronal debris and FGF-2 treatment: **, $P < 0.01$; ***, $P < 0.001$ (one-way ANOVA with Tukey's *post-hoc* test).

show that the concentration is around 50 pg/ml [47,48]. In a future study, we will attempt to clarify the effect of 100 ng/ml FGF2 *in vivo*. Taken together, the present study shows that FGF-2 from damaged neurons functions as help-me and eat-me signals. Targeting the FGF-2/FGFR3 pathway may give us clues for future therapeutic strategy against neurodegenerative diseases.

Conclusions

The present study shows that FGF-2 could be a key signaling molecule for crosstalk between degenerating neurons and microglia, and the FGFR3/ERK/Wnt signaling pathway in microglia contributes to the induction of neuroprotective function including migration and phagocytosis of neuronal debris. Therefore, FGF-2 from damaged neurons functions as help-me and eat-me signals to microglia.

Additional file

Additional file 1: Figure S1. FGF-2 inhibited the release of neurotoxic molecules from activated microglia. **Figure S2.** FGF-2 dose-dependently enhanced neuronal survival in the presence of microglia. **Figure S3.** FGF-2 increased CCL3 (MIP-1α) production in microglia. **Figure S4.** Effects of FGF-2 on microglial migration.

Abbreviations

aFGF2: anti-FGF2 neutralizing antibody; aFKN: anti-FKN neutralizing antibody; ANOVA: analysis of variance; BDNF: brain-derived neurotrophic factor; CNS: central nervous system; DIV: day *in vitro*; DMEM: Dulbecco's modified Eagle medium; DMSO: dimethyl sulfoxide; ELISA: enzyme-linked immunosorbent assay; ERK: extracellular signal-regulated kinase; FACS: fluorescence-activated cell sorting; FKN: fractalkine; FGF: fibroblast growth factor; FGFR: fibroblast growth factor receptor; GAPDH: glyceraldehydes-3-phosphate dehydrogenase; HFIP: 1,1,1,3,3,3-hexafluoro-2-propanol; IgG: immunoglobulin G; LPS: lipopolysaccharide; MS: multiple sclerosis; oAβ: oligomeric amyloid β; PD: pan-FGFR blocker; PET: polyethylene terephthalate; PVDF: polyvinylidene difluoride; RT-PCR: reverse transcriptase polymerase chain reaction; SDS: sodium dodecyl sulfate; SEM: standard error of the mean.

Competing interests

The authors declare that they have no competing interests.

Authors' contributions

MN conducted the ELISAs, microglial phagocytosis assay, FACS analysis, and statistical analysis, and drafted the manuscript. KT performed the RT-PCR experiments and helped draft the manuscript. BP and JK performed the cell culture and were involved in the conception of the study. YS and HT were also involved in the conception of the study. TM carried out the immunocytochemistry and statistical analysis. He was also involved in the conception and design of the study, and helped draft the manuscript. AS was also involved in the conception and design of the study, as well as in preparing the manuscript. All authors read and approved the final manuscript.

Acknowledgements

This study was supported by JSPS KAKENHI Grant Number 24659430, a grant from the Advanced Research for Medical Products Mining Programme of the National Institute of Biomedical Innovation (NIBIO), and grants from the Ministry of Health, Labour and Welfare of Japan.

Author details

[1]Department of Neuroimmunology, Research Institute of Environmental Medicine, Nagoya University, Furo-cho, Chikusa-ku, Nagoya 464-8601, Japan. [2]Present address: Department of Anatomy, Keio University School of Medicine, 35 Shinanomachi, Shinjuku-ku, Tokyo 160-8582, Japan.

Received: 23 January 2014 Accepted: 26 March 2014
Published: 16 April 2014

References

1. Mehta SL, Manhas N, Raghubir R: **Molecular targets in cerebral ischemia for developing novel therapeutics.** *Brain Res Rev* 2007, **54**:34–66.
2. Glass CK, Saijo K, Winner B, Marchetto MC, Gage FH: **Mechanisms underlying inflammation in neurodegeneration.** *Cell* 2010, **140**:918–934.
3. Gold SM, Mohr DC, Huitinga I, Flachenecker P, Sternberg EM, Heesen C: **The role of stress-response systems for the pathogenesis and progression of MS.** *Trends Immunol* 2005, **26**:644–652.
4. Chekeni FB, Elliott MR, Sandilos JK, Walk SF, Kinchen JM, Lazarowski ER, Armstrong AJ, Penuela S, Laird DW, Salvesen GS, Isakson BE, Bayliss DA, Ravichandran KS: **Pannexin 1 channels mediate 'find-me' signal release and membrane permeability during apoptosis.** *Nature* 2010, **467**:863–867.
5. Grimsley C, Ravichandran KS: **Cues for apoptotic cell engulfment: eat-me, don't eat-me and come-get-me signals.** *Trends Cell Biol* 2003, **13**:648–656.
6. Lu Z, Elliott MR, Chen Y, Walsh JT, Klibanov AL, Ravichandran KS, Kipnis J: **Phagocytic activity of neuronal progenitors regulates adult neurogenesis.** *Nat Cell Biol* 2011, **13**:1076–1083.
7. Ravichandran KS: **Find-me and eat-me signals in apoptotic cell clearance: progress and conundrums.** *J Exp Med* 2010, **207**:1807–1817.
8. Napoli I, Neumann H: **Microglial clearance function in health and disease.** *Neuroscience* 2009, **158**:1030–1038.
9. Kettenmann H, Hanisch UK, Noda M, Verkhratsky A: **Physiology of microglia.** *Physiol Rev* 2011, **91**:461–553.
10. Hanisch UK, Kettenmann H: **Microglia: active sensor and versatile effector cells in the normal and pathologic brain.** *Nat Neurosci* 2007, **10**:1387–1394.
11. Noda M, Suzumura A: **Sweepers in the CNS: microglial migration and phagocytosis in the Alzheimer disease pathogenesis.** *Int J Alzheimers Dis* 2012, **2012**:891087.
12. Aman A, Piotrowski T: **Wnt/β-catenin and Fgf signaling control collective cell migration by restricting chemokine receptor expression.** *Dev Cell* 2008, **15**:749–761.
13. Aman A, Piotrowski T: **Cell-cell signaling interactions coordinate multiple cell behaviors that drive morphogenesis of the lateral line.** *Cell Adh Migr* 2011, **5**:499–508.
14. Ma EY, Raible DW: **Signaling pathways regulating zebrafish lateral line development.** *Curr Biol* 2009, **19**:R381–R386.
15. Hossain WA, Morest DK: **Fibroblast growth factors (FGF-1, FGF-2) promote migration and neurite growth of mouse cochlear ganglion cells *in vitro*: immunohistochemistry and antibody perturbation.** *J Neurosci Res* 2000, **62**:40–55.
16. Clemente D, Ortega MC, Arenzana FJ, de Castro F: **FGF-2 and Anosmin-1 are selectively expressed in different types of multiple sclerosis lesions.** *J Neurosci* 2011, **31**:14899–14909.
17. Gehrmann J, Lannes-Vieira J, Wekerle H: **Differential expression of fibroblast growth factor-2 and receptor by glial cells in experimental autoimmune encephalomyelitis (EAE).** *Glia* 1996, **16**:93–100.
18. Riva MA, Molteni R, Lovati E, Fumagalli F, Rusnati M, Racagni G: **Cyclic AMP-dependent regulation of fibroblast growth factor-2 messenger RNA levels in rat cortical astrocytes: comparison with fibroblast growth factor-1 and ciliary neurotrophic factor.** *Mol Pharmacol* 1996, **49**:699–706.
19. Ganat Y, Soni S, Chacon M, Schwartz ML, Vaccarino FM: **Chronic hypoxia up-regulates fibroblast growth factor ligands in the perinatal brain and induces fibroblast growth factor-responsive radial glial cells in the sub-ependymal zone.** *Neuroscience* 2002, **112**:977–991.
20. Sleeman M, Fraser J, McDonald M, Yuan S, White D, Grandison P, Kumble K, Watson JD, Murison JG: **Identification of a new fibroblast growth factor receptor, FGFR5.** *Gene* 2001, **271**:171–182.
21. Logan A, Frautschy SA, Gonzalez AM, Baird A: **A time course for the focal elevation of synthesis of basic fibroblast growth factor and one of its high-affinity receptors (flg) following a localized cortical brain injury.** *J Neurosci* 1992, **12**:3828–3837.
22. Goddard DR, Berry M, Kirvell SL, Butt AM: **Fibroblast growth factor-2 induces astroglial and microglial reactivity *in vivo*.** *J Anat* 2002, **200**:57–67.
23. Aman A, Nguyen M, Piotrowski T: **Wnt/β-catenin dependent cell proliferation underlies segmented lateral line morphogenesis.** *Dev Biol* 2011, **349**:470–482.

24. Holnthoner W, Pillinger M, Groger M, Wolff K, Ashton AW, Albanese C, Neumeister P, Pestell RG, Petzelbauer P: **Fibroblast growth factor-2 induces Lef/Tcf-dependent transcription in human endothelial cells.** *J Biol Chem* 2002, **277**:45847–45853.
25. Noda M, Doi Y, Liang J, Kawanokuchi J, Sonobe Y, Takeuchi H, Mizuno T, Suzumura A: **Fractalkine attenuates excito-neurotoxicity via microglial clearance of damaged neurons and antioxidant enzyme heme oxygenase-1 expression.** *J Biol Chem* 2011, **286**:2308–2319.
26. Doi Y, Mizuno T, Maki Y, Jin S, Mizoguchi H, Ikeyama M, Doi M, Michikawa M, Takeuchi H, Suzumura A: **Microglia activated with the toll-like receptor 9 ligand CpG attenuate oligomeric amyloid β neurotoxicity in *in vitro* and *in vivo* models of Alzheimer's disease.** *Am J Pathol* 2009, **175**:2121–2132.
27. Mizuno T, Kurotani T, Komatsu Y, Kawanokuchi J, Kato H, Mitsuma N, Suzumura A: **Neuroprotective role of phosphodiesterase inhibitor ibudilast on neuronal cell death induced by activated microglia.** *Neuropharmacology* 2004, **46**:404–411.
28. Banno M, Mizuno T, Kato H, Zhang G, Kawanokuchi J, Wang J, Kuno R, Jin S, Takeuchi H, Suzumura A: **The radical scavenger edaravone prevents oxidative neurotoxicity induced by peroxynitrite and activated microglia.** *Neuropharmacology* 2005, **48**:283–290.
29. Suzumura A, Mezitis SG, Gonatas NK, Silberberg DH: **MHC antigen expression on bulk isolated macrophage-microglia from newborn mouse brain: induction of Ia antigen expression by γ-interferon.** *J Neuroimmunol* 1987, **15**:263–278.
30. Mizuno T, Kawanokuchi J, Numata K, Suzumura A: **Production and neuroprotective functions of fractalkine in the central nervous system.** *Brain Res* 2003, **979**:65–70.
31. Figueiredo C, Pais TF, Gomes JR, Chatterjee S: **Neuron-microglia crosstalk up-regulates neuronal FGF-2 expression which mediates neuroprotection against excitotoxicity via JNK1/2.** *J Neurochem* 2008, **107**:73–85.
32. Zhou Y, Sonobe Y, Akahori T, Jin S, Kawanokuchi J, Noda M, Iwakura Y, Mizuno T, Suzumura A: **IL-9 promotes Th17 cell migration into the central nervous system via CC chemokine ligand-20 produced by astrocytes.** *J Immunol* 2011, **186**:4415–4421.
33. Reuss B, von Bohlen und, Halbach O: **Fibroblast growth factors and their receptors in the central nervous system.** *Cell Tissue Res* 2003, **313**:139–157.
34. Masih-Khan E, Trudel S, Heise C, Li Z, Paterson J, Nadeem V, Wei E, Roodman D, Claudio JO, Bergsagel PL, Stewart AK: **MIP-1α (CCL3) is a downstream target of FGFR3 and RAS-MAPK signaling in multiple myeloma.** *Blood* 2006, **108**:3465–3471.
35. Choi DY, Toledo-Aral JJ, Lin HY, Ischenko I, Medina L, Safo P, Mandel G, Levinson SR, Halegoua S, Hayman MJ: **Fibroblast growth factor receptor 3 induces gene expression primarily through Ras-independent signal transduction pathways.** *J Biol Chem* 2001, **276**:5116–5122.
36. Katoh M, Katoh M: **Cross-talk of WNT and FGF signaling pathways at GSK3β to regulate β-catenin and SNAIL signaling cascades.** *Cancer Biol Ther* 2006, **5**:1059–1064.
37. Halleskog C, Mulder J, Dahlstrom J, Mackie K, Hortobagyi T, Tanila H, Kumar Puli L, Farber K, Harkany T, Schulte G: **WNT signaling in activated microglia is proinflammatory.** *Glia* 2011, **59**:119–131.
38. Drafahl KA, McAndrew CW, Meyer AN, Haas M, Donoghue DJ: **The receptor tyrosine kinase FGFR4 negatively regulates NF-kappaB signaling.** *PLoS One* 2010, **5**:e14412.
39. Sasaki T, Ito Y, Xu X, Han J, Bringas P Jr, Maeda T, Slavkin HC, Grosschedl R, Chai Y: **LEF1 is a critical epithelial survival factor during tooth morphogenesis.** *Dev Biol* 2005, **278**:130–143.
40. Garcia-Gonzalez D, Clemente D, Coelho M, Esteban PF, Soussi-Yanicostas N, de Castro F: **Dynamic roles of FGF-2 and Anosmin-1 in the migration of neuronal precursors from the subventricular zone during pre- and postnatal development.** *Exp Neurol* 2010, **222**:285–295.
41. Rottlaender A, Villwock H, Addicks K, Kuerten S: **Neuroprotective role of fibroblast growth factor-2 in experimental autoimmune encephalomyelitis.** *Immunology* 2011, **133**:370–378.
42. Paradiso B, Marconi P, Zucchini S, Berto E, Binaschi A, Bozac A, Buzzi A, Mazzuferi M, Magri E, Navarro Mora G, Rodi D, Su T, Volpi I, Zanetti L, Marzola A, Manservigi R, Fabene PF, Simonato M: **Localized delivery of fibroblast growth factor-2 and brain-derived neurotrophic factor reduces spontaneous seizures in an epilepsy model.** *Proc Natl Acad Sci USA* 2009, **106**:7191–7196.
43. Bovolenta R, Zucchini S, Paradiso B, Rodi D, Merigo F, Navarro Mora G, Osculati F, Berto E, Marconi P, Marzola A, Fabene PF, Simonato M: **Hippocampal FGF-2 and BDNF overexpression attenuates epileptogenesis-associated neuroinflammation and reduces spontaneous recurrent seizures.** *J Neuroinflammation* 2010, **7**:81.
44. Kiyota T, Ingraham KL, Jacobsen MT, Xiong H, Ikezu T: **FGF2 gene transfer restores hippocampal functions in mouse models of Alzheimer's disease and has therapeutic implications for neurocognitive disorders.** *Proc Natl Acad Sci USA* 2011, **108**:E1339–E1348.
45. Jones M, Tussey L, Athanasou N, Jackson DG: **Heparan sulfate proteoglycan isoforms of the CD44 hyaluronan receptor induced in human inflammatory macrophages can function as paracrine regulators of fibroblast growth factor action.** *J Biol Chem* 2000, **275**:7964–7974.
46. Kim J, Gale K, Kondratyev A: **Effects of repeated minimal electroshock seizures on NGF, BDNF and FGF-2 protein in the rat brain during postnatal development.** *Int J Dev Neurosci* 2010, **28**:227–232.
47. Mellergard P, Sjogren F, Hillman J: **Release of VEGF and FGF in the extracellular space following severe subarachnoidal haemorrhage or traumatic head injury in humans.** *Br J Neurosurg* 2010, **24**:261–267.
48. Mellergard P, Sjogren F, Hillman J: **The cerebral extracellular release of glycerol, glutamate, and FGF2 is increased in older patients following severe traumatic brain injury.** *J Neurotrauma* 2012, **29**:112–118.

doi:10.1186/1742-2094-11-76
Cite this article as: Noda *et al.*: FGF-2 released from degenerating neurons exerts microglial-induced neuroprotection via FGFR3-ERK signaling pathway. *Journal of Neuroinflammation* 2014 **11**:76.

Behavioural Brain Research 268 (2014) 88–93

Contents lists available at ScienceDirect

Behavioural Brain Research

journal homepage: www.elsevier.com/locate/bbr

Research report

Fingolimod increases brain-derived neurotrophic factor levels and ameliorates amyloid β-induced memory impairment

Kazuya Fukumoto[a], Hiroyuki Mizoguchi[a,*], Hideyuki Takeuchi[b], Hiroshi Horiuchi[b], Jun Kawanokuchi[b], Shijie Jin[b], Tetsuya Mizuno[b], Akio Suzumura[b]

[a] Futuristic Environmental Simulation Center, Research Institute of Environmental Medicine, Nagoya University, Furo-cho, Chikusa-ku, Nagoya 464-8601, Japan
[b] Department of Neuroimmunology, Research Institute of Environmental Medicine, Nagoya University, Furo-cho, Chikusa-ku, Nagoya 464-8601, Japan

HIGHLIGHTS

- Fingolimod ameliorated memory and learning impairments in amyloid β-injected mice.
- Fingolimod restored normal levels of BDNF in cerebrum of amyloid β-injected mice.
- Fingolimod may be a promising therapeutic agent for Alzheimer's disease.

ARTICLE INFO

Article history:
Received 7 January 2014
Received in revised form 26 March 2014
Accepted 31 March 2014
Available online 5 April 2014

Keywords:
Fingolimod
Alzheimer's disease
Amyloid β
Brain-derived neurotrophic factor

ABSTRACT

Alzheimer's disease is a progressive neurodegenerative disorder. Amyloid β, a neurotoxic protein, causes disruption of hippocampal synaptic plasticity, and induces cognitive impairment in Alzheimer's disease. We previously revealed that fingolimod, a new oral immunosuppressant used to treat multiple sclerosis, ameliorates oligomeric amyloid β-induced neuronal damage via up-regulation of neuronal brain-derived neurotrophic factor (BDNF). Here, we showed that oral administration of fingolimod ameliorated the impairment in object recognition memory and associative learning in mice injected with amyloid β. This effect was associated with restoration of normal BDNF expression levels in the cerebral cortices and hippocampi, suggesting that neuroprotection was mediated by up-regulation of neuronal BDNF levels. Therefore, fingolimod may provide therapeutic effects in patients with Alzheimer's disease.

1. Introduction

Alzheimer's disease, the most common age-related neurodegenerative disorder in humans, is characterized by deterioration of cognitive and mental functions. The formation of extracellular deposits of amyloid β (Aβ) peptide, leading to the formation of neuritic plaques and neurofibrillary tangles in the cortex and hippocampus, is a prominent pathological feature of Alzheimer's disease [1,2]. Aβ is produced from amyloid precursor protein through sequential cleavages and secreted to the extracellular space. Aβ is strongly fibrillogenic: soluble oligomeric Aβ (oAβ) monomers gradually convert to oligomers and ultimately to insoluble fibrils. Recent studies have shown that oAβ is more neurotoxic than fibrillar Aβ [3,4]. Aβ-mediated neurotoxicity has been extensively demonstrated both in vivo and in vitro studies. oAβ induces neuronal oxidative stress by activating *N*-methyl-D-aspartate (NMDA) receptors, leading to neuronal death [5]. We also have demonstrated that the intracerebroventricular (i.c.v.) injection of Aβ induces cognitive deficits [6] as well as impairment of the cholinergic system and down-regulation of brain-derived neurotrophic factor (BDNF); these changes play important roles in cognitive and morphological deficits associated with aging and neurodegenerative diseases [7,8].

Fingolimod is an oral immunosuppressant, which has been recently approved for treatment of multiple sclerosis [9–12]. In rats, orally administered fingolimod localizes to white matter in the central nervous system (CNS), preferentially along myelin sheathes [13]. The drug was synthesized by modifying myriocin, which is derived from *Isaria sinclairii* [14]. Fingolimod is phosphorylated in vivo by sphingosine kinase to form the active metabolite. After binding to sphingosine-1-phosphate (S1P) receptor 1 ($S1P_1$) on the

Abbreviations: oAβ, oligomeric amyloid β; BDNF, brain-derived neurotrophic factor; NORT, novel-object recognition test; S1P, sphingosine-1-phosphate; S1PR, sphingosine-1-phosphate receptor; Trk, tropomyosin-related kinase.

* Corresponding author. Tel.: +81 52 789 3929; fax: +81 52 789 3999.
E-mail address: h-mizo@riem.nagoya-u.ac.jp (H. Mizoguchi).

http://dx.doi.org/10.1016/j.bbr.2014.03.046
0166-4328/

surface of lymphocytes, phosphorylated fingolimod induces $S1P_1$ internalization; as a result, the lymphocytes can no longer egress from lymphoid tissues. Thus, fingolimod acts as a functional antagonist $S1P_1$ and reduces the migration of immune cells into the CNS, thereby providing therapeutic effects against subsequent neuroinflammation [15–17].

S1P receptors (S1PRs) are widely expressed in various CNS cell types, including neurons, astrocytes, microglia, and oligodendrocytes [18]. Phosphorylated fingolimod can bind to all S1PR subtypes ($S1P_1$, $S1P_3$, $S1P_4$, and $S1P_5$) but $S1P_2$ [19,20]. Previous studies demonstrated that phosphorylated fingolimod directly promotes remyelination mediated by oligodendrocyte progenitor cells [21] and enhances neuroprotective effects through astrocyte $S1P_1$ modulation [22]. Recently, we showed that phosphorylated fingolimod binds to $S1P_1$ receptors, resulting in down-regulation of pro-inflammatory cytokine production by activated microglia, up-regulation of microglial production of neurotrophic factors, and augmentation of the neuroprotective effects of microglia [23]. Moreover, we also showed that phosphorylated fingolimod directly affects neurons and prevents oAβ-induced neuronal damage via up-regulation of neuronal BDNF production [24].

In this study, we investigated the efficacy of fingolimod on cognitive impairment in a mouse model of Alzheimer's disease induced by i.c.v. injection of oAβ. Fingolimod significantly ameliorated cognitive impairments, and this effect was accompanied by restoration of normal BDNF production in the brain. Our findings suggest that fingolimod may have therapeutic potential for treatment of Alzheimer's disease.

2. Materials and methods

2.1. Animals

Male C57BL/6J mice (7–8 weeks old; weighing 40 ± 5 g at the beginning of the experiments) were obtained from Japan SLC (Hamamatsu, Japan). The animals were housed in plastic cages and kept in a regulated environment (23 ± 1 °C; 50 ± 5% humidity) with a 12-h light – dark cycle (lights on at 9:00 am). Food (CE-2, CLEA Japan) and tap water were available ad libitum. All experiments were performed in accordance with the Guidelines for Animal Experiments of Nagoya University; the Guiding Principles for the Care and Use of Laboratory Animals approved by the Japanese Pharmacological Society; and the United States National Institutes of Health Guide for the Care and Use of Laboratory Animals.

2.2. Peptides and drugs

Soluble oligomeric Aβ1-42 (oAβ1-42) was prepared as described previously [4,25]. Briefly, synthetic human Aβ1-42 (Peptide Institute, Osaka, Japan) was dissolved in 100% 1,1,1,3,3,3-hexafluoro-2-propanol and dried to completely remove the solvent. The obtained film was resuspended in dimethyl sulfoxide and diluted with Dulbecco's Modified Eagle Medium/F12 (Invitrogen, Carlsbad, CA, USA) at a concentration of 100 μM. This solution was incubated at 4 °C for 24 h to obtain oAβ. A final concentration of 300 μM oAβ1-42 was used for all experiments. Oligomerization of oAβ was characterized by Western blotting.

All peptides were injected as described previously [26] and summarized as follows. A microsyringe with a 28-gauge stainless-steel needle was used for all experiments. Mice were anesthetized using 50 mg/kg sodium pentobarbital i.p. before stereotaxic implantation of a microinjection cannula into the right lateral ventricle (anteroposterior +0.3 mm, mediolateral +1.0 mm from the bregma, and dorsoventral −2.5 mm from the skull) according to the method of Franklin and Paxinos (1997). oAβ1-42 (300 pmol) was i.c.v. injected in a volume of 3 μL for 3 min. The same volume of oAβ42-1 (a peptide with identical amino-acid composition to oAβ1-42, but with the reverse sequence) was injected as a control. Mice exhibited normal behavior within 1 min after the injection. Behavioral assessments were performed starting at 5 days after injection (day 5, Fig. 1A).

Fingolimod, kindly provided by Novartis Pharma AG (Basel, Switzerland), was dissolved in distilled water. Fingolimod or vehicle was administered at a dose of 1 mg/kg by oral gavage needle, once a day for 14 days after oAβ injection, as previously described (Fig. 1A) [22].

2.3. Novel-object recognition test (NORT)

The NORT was carried out as described previously [27,28]. The experimental apparatus consisted of a Plexiglas open-field box ($l \times w \times h$: 30 cm × 30 cm × 35 cm), with a sawdust-covered floor. The apparatus was located in a sound-attenuated room and illuminated with a 20 W bulb.

The NORT procedure consisted of three sessions: habituation, training, and retention. Each mouse was individually habituated to the box with 10 min of exploration in the absence of objects for 3 consecutive days (habituation sessions, days 5–7). During the training session, two novel objects were symmetrically fixed to the floor of the box, 8 cm from the walls, and each animal was allowed to explore in the box for 10 min (day 8). The objects were constructed from a golf ball, a wooden column, and a wooden triangle pole, which were different in shape and color but similar in size. An animal was considered to be exploring the object when its head was facing the object or it was touching or sniffing the object. The time spent exploring each object was recorded. After training, mice were immediately returned to their home cages. During the retention sessions, the animals were placed back into the same box 24 h after the training session (day 9), but one of the familiar objects used during training had been replaced with a novel object. The animals were then allowed to explore freely for 5 min, and the time spent exploring each object was recorded. Throughout the experiments, novel and familiar objects were of similar physical complexity and emotional valence. In the retention session, the preference index was defined as the ratio of the amount of time spent exploring the novel object to the total time spent exploring both objects; this metric was used to measure cognitive function. In the training session, the preference index was defined as the ratio of the time spent exploring the object that was replaced by the novel object in the retention session to the total exploration time.

2.4. Conditioned-fear memory test

Mice were divided into two groups according to experimental schedule (Fig. 1A). Fear conditioning test for group 1 was performed on day 12–13, and the test for group 2 was performed on day 13–14. Fear conditioning tests were performed as previously described [26,29,30] with minor modifications. Freezing behavior, during which the mouse's head, arms, and legs did not move, was timed using a stopwatch. To measure the basal freezing response (preconditioning phase), mice were individually placed in a transparent Plexiglas conditioning cage (30 cm × 30 cm × 35 cm) for 2 min. For training (conditioning phase, day 12 for group 1 or day 13 for group 2), mice were placed in the conditioning cage and subjected to the conditioned stimulus (a 15-s tone at 80 dB). During the last 5 s of the tone stimulus, a 0.6-mA foot shock was delivered as the unconditioned stimulus via a shock generator (BrainScience Idea Co., Osaka, Japan). This procedure was repeated six times at 15-s intervals, and mice were left in place for an additional 1 min after the final unconditioned stimulus. Contextual and cued tests were carried out 1 day after fear conditioning (day 13 for group 1 or day